Chapter 8
Neutrino Detectors

Leslie Camilleri

After a brief introduction describing the many sources of neutrinos, this article will describe the various detector techniques that are being used to observe neutrinos of energies ranging from a few MeV to hundred's of GeV.

8.1 Historical Introduction

In 1930 in order to explain the continuous energy spectrum of electrons emitted in beta decay, Pauli postulated [1] that these electrons were emitted together with a light neutral particle. This particle was subsequently named the neutrino. Their actual observation had to wait until 1953 when Reines and Cowan recorded [2] interactions of anti(electron)neutrinos emitted by a reactor in a cadmium doped liquid scintillator detector. Since then, in addition to the ν_e, two other flavours of neutrinos were observed, the ν_μ and ν_τ. The ν_μ, which is produced in $\pi \rightarrow \mu$ decay, was proved to be different [3] from the ν_e in an experiment at Brookhaven using thick-plate optical spark chambers. The ν_τ, companion of the τ lepton, was observed [4] at Fermilab in an emulsion cloud chamber detector consisting of iron plates interleaved with sheets of photographic emulsions. Although until recently neutrinos were thought to be massless and were described as such in the Standard Model, in the past decade they have been found to be massive [5, 6]. Furthermore each of the three flavour states mentioned above consists of a superposition of three mass states of unequal masses leading to oscillations of one flavour into another under the appropriate conditions. The characteristics of these oscillations depend on three mixing angles θ_{13}, θ_{12} and θ_{23} as well as on the difference of the square of the 3

L. Camilleri (✉)
Nevis Labs, Columbia University, Irvington-on-Hudson, NY, USA
e-mail: camil@nevis.columbia.edu

C. W. Fabjan, H. Schopper (eds.), *Particle Physics Reference Library*,
https://doi.org/10.1007/978-3-030-35318-6_8

neutrino masses, Δm^2_{12} referred to as the solar mass difference as it is of importance in oscillations of solar neutrinos, $\Delta m^2_{13} \sim \Delta m^2_{23}$ referred to as the atmospheric mass difference as it drives oscillations of neutrinos produced in the atmosphere through the decay of mesons produced in cosmic ray interactions. The flavour of interacting neutrinos can only be determined if the interaction is via a charged current. In these, the ν_e, ν_μ and ν_τ respectively produce a negative electron, muon or τ lepton in the final state. Antineutrinos produce the corresponding positive charged lepton.

8.2 Sources of Neutrinos and Their Characteristics

Naturally occurring neutrinos and man-made neutrinos are produced through several different processes. Nature provides us with solar neutrinos emitted by the sun, atmospheric neutrinos produced by the interaction of cosmic rays in the atmosphere, cosmological neutrinos produced by a variety of deep space violent events, geological neutrinos produced by nuclear decays in the earth core as well as neutrinos produced in beta decay. Man made neutrinos are produced by nuclear reactors or by specially designed beams at accelerators or by highly radioactive sources. These processes are briefly described below.

8.2.1 Solar Neutrinos

They are emitted in nuclear reactions occurring in the sun [7]. The three main reactions are $\mathrm{p} + \mathrm{p} \rightarrow \mathrm{d} + \mathrm{e}^+ + \nu_e$, emitting a continuous spectrum of neutrinos with an end point at 0.4 MeV, $\mathrm{e} + {}^7\mathrm{Be} \rightarrow {}^7\mathrm{Li} + \nu_e$ with a monochromatic spectrum at 0.862 MeV and ${}^8\mathrm{B} \rightarrow {}^8\mathrm{Be}^* + \mathrm{e}^+ + \nu_e$ also with a continuous spectrum with an end point at 15 MeV. Their total flux on earth is $6.4 \times 10^{+10}\,\mathrm{cm}^{-2}\mathrm{s}^{-1}$.

8.2.2 Atmospheric Neutrinos

Atmospheric neutrinos [8] are produced in the decays of π and K mesons produced in the interactions of cosmic rays in the upper atmosphere. Their energy ranges over several orders of magnitude up to hundreds of GeV. They are observed either coming from above or from below and in the latter case they will have traversed the earth. This allows us to observe them from a few kilometers to about 13,000 km from their production point, thus providing us with very different baselines over which to study oscillations. These predominantly ν_e and ν_μ neutrinos are usually observed through their charged current interactions respectively producing electrons or muons.

8.2.3 Cosmological Neutrinos

The study of cosmological neutrinos [9] at the TeV scale is in its infancy. Their very low rate necessitates extremely large detectors. This has led to the use of naturally occurring detection media such as lake or sea water and Antarctic ice. The Cerenkov light or radio waves emitted by charged particles produced in their interactions in the medium are recorded, respectively, in strings of photomultiplier tubes or antennas.

8.2.4 Reactor Neutrinos

Nuclear reactors are an abundant source of antineutrinos, 6 $\bar{\nu}_e$ per nuclear fission on average, resulting in a flux of 1.8×10^{20} per GW thermal energy, emitted isotropically. The standard method to study them [10] is to observe the Inverse Beta Decay (IBD) reaction $\bar{\nu}_e + p \rightarrow e^+ + n$ in a hydrogen-rich liquid scintillator detector. In addition to observing photons emitted as a result of the positron annihilation, the neutron can be detected by recording photons emitted by the neutron capture in the scintillator.

8.2.5 Accelerator Neutrinos

Accelerator neutrinos are produced [11] by the decay of π and K mesons themselves produced by the interaction of a proton beam on a target as illustrated in Fig. 8.1. The target must be thick enough along the beam to maximize the proton interaction probability and yet thin enough to minimize the reinteraction probability and multiple scattering of the produced mesons such as to produce as high an energy and as focussed a beam as possible. The usual target geometry consists of a series of thin rods of low Z material such as carbon or beryllium separated by a few cms but in line with the proton beam. The mesons are then focussed by a system of toroidal magnets. These, referred to as horns [12], consist of two concentric current sheets, parabolically shaped that provide a toroidal magnetic field. Its strength is inversally proportional to the radial displacement from the beam axis and the integral is such as to bend more the particles that are further away from the beam thus providing a near parallel beam. A second horn is usually provided such as to compensate for

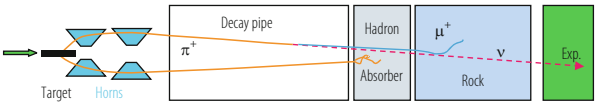

Fig. 8.1 The principle of an accelerator produced neutrino beam

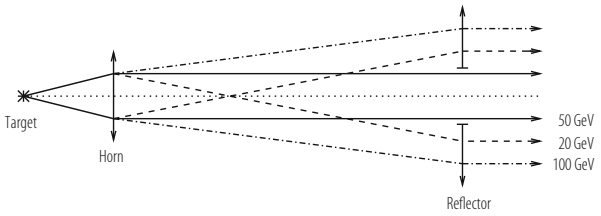

Fig. 8.2 The principle of horn focusing of mesons in a neutrino beam

over-focussed and under-focussed particles as shown in Fig. 8.2. The particles then enter a long evacuated decay tunnel in which $\pi \rightarrow \mu\nu_\mu$, $K \rightarrow \mu\nu_\mu$ and $K \rightarrow \pi e\nu_e$ decays occur producing a predominantly ν_μ beam with an admixture of $\sim$1% of ν_e. Focussing positive mesons produces a neutrino beam whereas focussing negative mesons, achieved by a reversal of the polarity of the horns, produces an antineutrino beam.

An alternative to the horns is a system of bending magnets and quadrupoles. Such a technique [13] has been used in the Sign Selected Quadrupole Train, SSQT, neutrino beam at Fermilab. Its performance is described in [14]. An advantage of this technique is that the neutrino beam not being along the axis of the proton beam, ν_e from K°_L decays will not enter the detector since their parents will not be deflected. This is a distinct advantage in oscillation experiments looking for ν_e appearance in a ν_μ beam in which the intrinsic ν_e background is irreducible.

The above techniques produce a beam with a broad energy spectrum, referred to as a broad band beam. A narrower range of neutrino energies is sometimes desirable. Such narrow band beams are obtained by first momentum-selecting the parent pions and kaons before they decay using standard beam optics methods, thus reducing the range of neutrino energies. Furthermore, the neutrino energy can be deduced on an event by event basis as it is related to the neutrino production angle and this can be computed from the radial position of the event within the detector. The uncertainty on the energy depends on the momentum and angular spread of the meson beam and on the length of the decay channel. It is typically 5–20%. The intensity of these narrow band beams is necessarily lower than that of broad band beams.

Another way to expose the detector to neutrinos with a given narrow energy spectrum is to place the detector at an off-axis angle to the beam [15]. The kinematics of pion decay, shown in Fig. 8.3 are such that neutrinos observed at a non-zero angle to the proton beam have an approximately unique momentum irrespective of the momentum of their parent meson. Furthermore the value of this unique momentum depends on the off-axis angle, thus allowing a detector to be exposed to the neutrino momentum required by the physics under investigation by placing it at the appropriate angle.

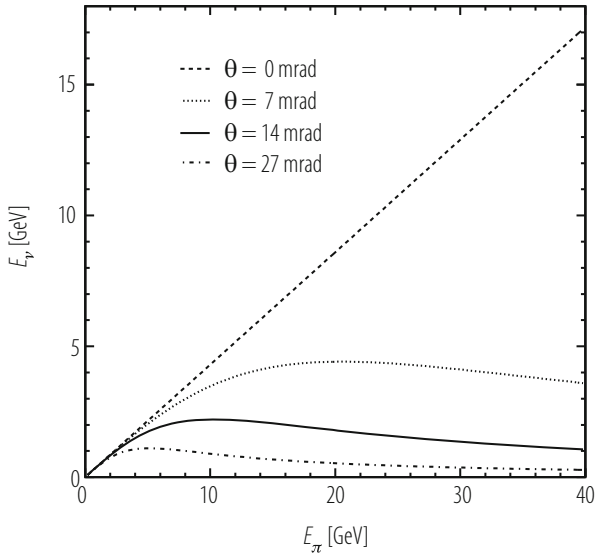

Fig. 8.3 The correlation between the pion momentum and its decay neutrino momentum, plotted for several neutrino directions relative to the proton beam axis

An accelerator neutrino beam can also, potentially, contain ν_τ's. These are produced through the production of D_s mesons in the initial proton interactions and their subsequent decays $D_s \rightarrow \tau\nu_\tau$ followed by $\tau \rightarrow \nu_\tau + \ldots$. However in most accelerator beams the ν_τ content is negligible since the D_s production cross section is small at existing energies. One notable exception will be discussed in Sect. 8.3.4.

The semi-leptonic decays of charmed particles have also been used to produce neutrinos. In this case, because of the very short lifetime of charm, a decay tunnel is unnecessary. The beam is produced in a so-called beam dump [16], in which the incident proton beam and secondary pions and kaons are absorbed before they can decay. At CERN, the beam dump [17] was made of copper disks that could be separated thus altering its density between 3 and $9\,\mathrm{g}\cdot\mathrm{cm}^{-3}$. The normal neutrino flux from π and K decays was reduced by about 3 orders of magnitude. Since charm is produced in pairs in proton interactions, the beam contains an approximately equal amount of neutrinos and antineutrinos, the only difference being due to π and K mesons decays occurring before these mesons are absorbed. Furthermore, because of the equal $e\nu_e$ and $\mu\nu_\mu$ decay probabilties of charm an equal number of ν_e and ν_μ are present in the beam. In this context, it is interesting to note [18] that hadronic colliders, and in particular LHC, produce a large quantity of charm and beauty particles in the forward directions, resulting in two well collimated neutrino beams emerging from each interaction region.

8.3 Detection Techniques

Because of the small interaction cross section of neutrinos, neutrino detectors must be massive. The exception is detectors addressing coherent neutrino interactions for which the cross section is orders of magnitude larger than for other neutrino interactions and which will be addressed in Sect. 8.3.1. The nature of these massive detectors depends on the physics being addressed. It usually involves observing the resulting hadronic part of an interaction and, if a charged current interaction, the observation of a charged lepton. If the physics merely requires the measurement of the total neutrino energy, a calorimetric detector suffices. If individual particles must be measured, then a more sophisticated tracking device is needed. The measurement of a final state muon is usually accomplished in a fairly straightforward way with magnetized iron because of the muon penetrating nature. A final state electron is more difficult to measure, especially its charge, because of bremsstrahlung and showering as it propagates through material. Neutrino detectors must then necessarily be of several types. Techniques must be suitable to detect neutrinos of energies ranging from a few MeV to about a PeV. They must be fine-grained enough to measure electrons, identify individual particles and observe secondary vertices of τ's or charmed particles or heavy enough to produce large number of interactions using calorimetric techniques. It is evident that neutrino detectors use most of the detecting techniques used in particle physics. They will be outlined in the following sections.

8.3.1 Totally Active Scintillator Detectors

Scintillator detectors can either use liquid or solid scintillator. If liquid is used the detector consists of either a single large tank or of tubes filled with liquid. Solid scintillator detectors usually consist of strips. The first neutrino detector [2] used by Reines and Cowan was intended to observe the interaction of reactor antineutrinos of a few MeV. The observation was made, as in subsequent reactor experiments, using the IBD reaction $\bar{\nu}_e + p \rightarrow e^+ + n$ and using a detector consisting of liquid scintillator viewed by photomultipliers. In addition to observing light emitted from the positron annihilation, the neutron can be detected by also observing photons emitted by the neutron capture in the hydrogen of the scintillator. In order to enhance the neutron capture cross section, they added cadmium to the scintillator. They observed an excess of events when the reactor was in operation leading to the first detection of (anti)neutrino interactions and a subsequent Nobel prize. This technique is still being applied to this day [10], albeit with some refinements. Several recent experiments which will be described below, used it to search for $\bar{\nu}_e$ oscillations to another flavour in the domain of the atmospheric $\Delta m^2, 2.5 \times 10^{-3}\,\mathrm{eV}^2$. Because of the low energy of reactor $\bar{\nu}_e$'s, $\bar{\nu}_\mu$'s or $\bar{\nu}_\tau$'s that they potentially oscillate to cannot be observed through their charged current

interactions since it is energetically impossible to produce μ's or τ's. Oscillations can then only be observed through the disappearance technique resulting in a reduction and distortion of the expected $\bar{\nu}_e$ spectrum. Given the energy of reactor $\bar{\nu}_e$'s (a few MeV) and the value of the atmospheric Δm^2, CHOOZ [19] was located 1000 m from a reactor complex in order to be near oscillation maximum. It used a single large tank of liquid scintillator and was subjected to a cosmic muon rate of $0.4\,\mathrm{m}^{-2}\mathrm{s}^{-1}$. One of the major backgrounds in this type of experiment is the background generated by cosmic ray muons. The first line of defense is to place the detector underground, at a depth of 300 m water equivalent (m.w.e) in the case of CHOOZ. A muon traversing the detector does not, in itself, simulate a signal event because the large amount of energy deposited can be well identified. However neutrons produced by muons traversing dead areas of the detector or the surrounding rock can elastically scatter on a proton, causing the proton and the subsequent neutron capture to simulate the signature of a reactor event. This background can be eliminated by vetoing on the passage of a nearby muon. In addition cosmic muons can produce long lived isotopes such as ^{6}He and ^{9}Li which subsequently can beta decay producing an electron and a neutron, thus simulating an antineutrino event. This background cannot be eliminated by vetoing on the passage of a muon because of the long lifetime of these decays (178 ms in the case of ^{9}Li) which would introduce an inordinate dead time. It must be estimated and subtracted. Palo Verde [20] was located at a shallower depth of 32 m.w.e. and chose to use acrylic cells filled with liquid scintillator. This extra segmentation was needed to reduce the larger muon induced neutron background caused by the larger cosmic muon flux of $22\,\mathrm{m}^{-2}\mathrm{s}^{-1}$ at this depth. Instead of cadmium, these experiments have been using a 0.1% admixture of gadolinium with a large neutron absorption cross section leading to an 84% capture fraction. Absorption in gadolinium leads to the emission of gamma rays with a total energy of 8 MeV, within $\sim$30 µs and $\sim$6 cm of the positron annihilation, thus providing a well recognizable delayed coincidence. The CHOOZ target scintillator consisted of 50% by volume Norpar-15 [21] and IPB + hexanol (also 50% by volume). The wave-length shifters were p-PTP and bis-MSB (1 g/l). The gadolinium was introduced as a solution of $Gd(NO_3)_3$ in hexanol. Because of oxygenation of the nitrate the 4 m light attenuation length in the scintillator decreased with time at a rate of $(4.2 \pm 0.4) \cdot 10^{-3}$ per day. This required a careful monitoring of the scintillator transparency using calibration sources. The light yield was 5300 photons/MeV.

The observation of a modification of the expected $\bar{\nu}_e$ spectrum necessitates a very precise knowledge of the antineutrino flux emitted by the reactor as well as of the antineutrino interaction cross section. They failed to observe a disappearance of antineutrinos and the limit set on this oscillation was governed by these sources of systematics uncertainty. In order to overcome these limitations more recent reactor oscillation experiments use a second identical detector located close to the reactor in order to measure the expected interaction rate before the neutrinos have a chance to oscillate. The detector used by one such experiment, Double Chooz [22], located at the same location as CHOOZ but using, in addition, a near detector placed at 410 m from the reactors, will be described as an example. The scintillator, amounting to

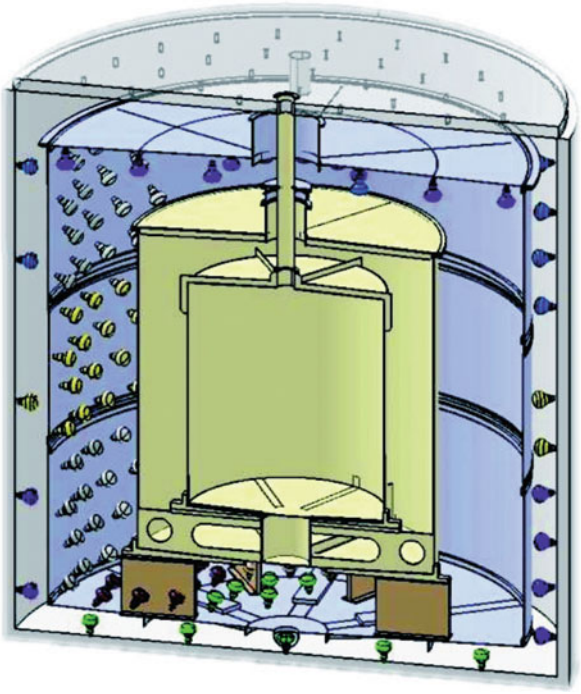

Fig. 8.4 The Double Chooz detector

10 tons, is housed in a central tank, Fig. 8.4, consisting of a clear acrylic. It is surrounded by a gamma catcher consisting of undoped liquid scintillator housed in a second acrylic shell that provides additional gamma detection probability for interactions occurring near the boundary of the central tank. A third envelope consisting of stainless steel holds the photomultipliers that view the two scintillator volumes through the acrylic shells. A buffer consisting of mineral oil fills the space between the stainless steel shell and the acrylic shell of the gamma catcher. It serves the purpose of absorbing any radioactivity emitted by the photomultipliers. In order to veto on cosmic muons the photomultiplier shell is itself surrounded by yet another scintillator volume housed in a final outer shell that also holds a second set of photomultipliers viewing this inner veto layer. Lastly, planes of scintillator counters cover the ceiling of the detector cavern, to identify more muons that traverse the surrounding material and are a potential source of neutrons. The scintillator chosen for the target is a 20/80 mixture of phenyl-xylelethane (PXE)/dodecane with 0.1% gadolinium doping introduced as a dipivaloymethane molecule, $Gd(dpm)_3$. This has demonstrated long term stability. With PPO and Bis-MSB as fluors the mixture has an attenuation length greater than 5 m at 450 nm and a light yield of 7000 photons/MeV resulting in 200 detected photoelectrons/MeV. The positron detection

threshold is less than 700 keV, well below the threshold of 1.022 MeV of the inverse beta decay reaction.

Calibration of the detector is required to determine, in both detectors, the efficiency for observing the inverse beta decay reaction, the energy scales for positrons, neutrons and gamma, the timing of the photomultipliers and the light transport properties. To this end gamma sources, neutron sources and laser light flashers are used and deployed throughout the detector volumes in order to map out the relevant parameters. In the target this is done with an articulated arm at the end of which is mounted the calibrating device, the position of which is determined by the length and azimuthal position of the arm. In the gamma catcher a guide tube into which a source can be inserted at the end of a wire is used. The geometry of the tube and the wire length determine the position of the source.

Whereas Double Chooz was the first to report a hint for a non-zero θ_{13}, two experiments have since produced the best measurements of this angle. They use the same concept as Double Chooz but have used either a larger neutrino flux (RENO [23]) or more detectors and more flux (Daya Bay [24]). RENO, in South Korea, is exposed to the flux of 6 reactors in a row totalling 16.4 GW_{th}. Its far detector is 168 m underground and 1380 m from the central reactor whereas its near detector is 46 m underground and 290 m from the reactor line. Its inner target weighs 15.4 tons and is viewed by 340 photomultipliers. Daya Bay, in China, uses eight identical detectors and is located near three reactor complexes Daya Bay, Ling Ao I and II, a total of 17.4 GW_{th}. Its far detector hall is 324 m underground, 1540 m from Ling Ao and 1910 m from Daya Bay and houses four detectors. One near detector hall 363 m from the Daya Bay complex and another one about 500 m from the Ling Ao complex each house 2 detectors. Each detector includes a 20 ton neutrino target viewed by 192 8″ photomultipliers. Their inner vetos are tanks of water in which Cerenkov light is viewed by photomultipliers. The Daya Bay energy resolution is $\sigma_E/E = 7.5\%/\sqrt{E}$. Using a variety of radioactive sources they are able to determine the absolute neutrino energy scale to 1% and the relative energy scale between detectors to <0.2%. The relative detection efficiency uncertainty was 0.13% and was substantiated by comparing rates of detectors in the same hall. Table 8.1 compares the systematic uncertainties achieved in Daya Bay to the ones in the CHOOZ single detector experiment demonstrating the effectiveness of a multiple detector and multiple location experiment. It should be noted that all three experiments have observed a structure in the positron energy distribution between 4 and 6 MeV when compared to Monte Carlo predictions based on the present understanding of a reactor neutrino flux. This structure is also seen in their near detectors (see for instance [25]) and its amplitude is proportional to the reactor flux. It is therefore believed to be due to our lack of complete understanding of the complex origin of a reactor neutrino flux.

KamLAND [26] is also an experiment observing reactor antineutrinos but studies oscillations in the domain of the solar $\Delta m^2, 7.5 \times 10^{-5}\,\mathrm{eV}^2$, and is therefore situated at an average distance of about 180 km from 53 Japanese power reactors to compensate for the much smaller Δm^2. The same reaction and technique as described above are used. However to observe enough events at this distance

Table 8.1 The Daya Bay systematic uncertainties compared to the ones in CHOOZ

Variable	CHOOZ [%]	Daya Bay [%]
ν flux and cross section	1.9	–
Reactor power	0.7	–
Energy per fission	0.6	–
Number of protons	0.3	0.03
H/C ratio and Gd concentration	1.2	0.1
Spatial effects	1.0	0.02
Live time	–	0.01
Analysis cuts	1.5	0.082
Total	2.7	<0.13

a detector consisting of 1 kiloton of liquid scintillator had to be used. The scintillator is housed in a 13 m diameter transparent nylon balloon suspended in non-scintillating oil acting as a buffer and viewed by 1879 photomultipliers. This inner detector is surrounded by a 3.2 kiloton water Cerenkov counter which has the dual purpose of reducing γ rays and neutrons from the surrounding rock and of detecting cosmic ray muons. As well as measuring the oscillation pattern as a function of L/E of reactor neutrinos within their detector, KamLAND also made a measurement of geological neutrinos [27].

The KamLAND detector would also be used in the IsoDAR project [28] searching for sterile neutrinos through $\bar{\nu}_e$ disappearance at a Δm^2 of $\sim$1 eV^2. A 60 MeV cyclotron would be placed a few meters from the surface of KamLAND and 16.5 m from its centre, Fig. 8.5. The cyclotron would accelerate H_2^+ ions (a hydrogen molecule with one electron removed) as the single charge for two protons of H_2^+ reduces the repulsive force within a bunch and hence minimizes the effect of space charge blow up of the beam which in turn keeps beam loss down. A high current source, currently under commissioning, would produce the H_2^+ ions which would be bunched with a radio-frequency quadrupole placed vertically above the centre of the cyclotron. The bunched ions would be bent electrostatically into the plane of the cyclotron. After 96 turns they would be extracted with a thin septum, stripped and transported 50 m, resulting in 10 mA of protons impinging on a beryllium target placed near the KamLAND detector. Neutrons produced in this target stream through a sleeve consisting of small beryllium spheres surrounded by highly enriched (99.995%) ^{7}Li. A graphite reflector surrounds the target and sleeve. The neutrons captured by the lithium produce ^{8}Li which subsequently decays producing $\bar{\nu}_e$'s entering the KamLAND detector in which they can be detected via IBD. The (12 cm/$\sqrt{E_{MeV}}$) spatial resolution and (6.4%/$\sqrt{E_{MeV}}$) energy resolution of KamLAND coupled with the detector size allows the observation of event rate oscillations as a function of L/E within KamLAND in addition to an overall disappearance of $\bar{\nu}_e$'s.

Reactor complexes are next planned to be used as sources of antineutrinos to illuminate two larger versions ($\sim$10 kilotons up from $\sim$10 tons) of the current

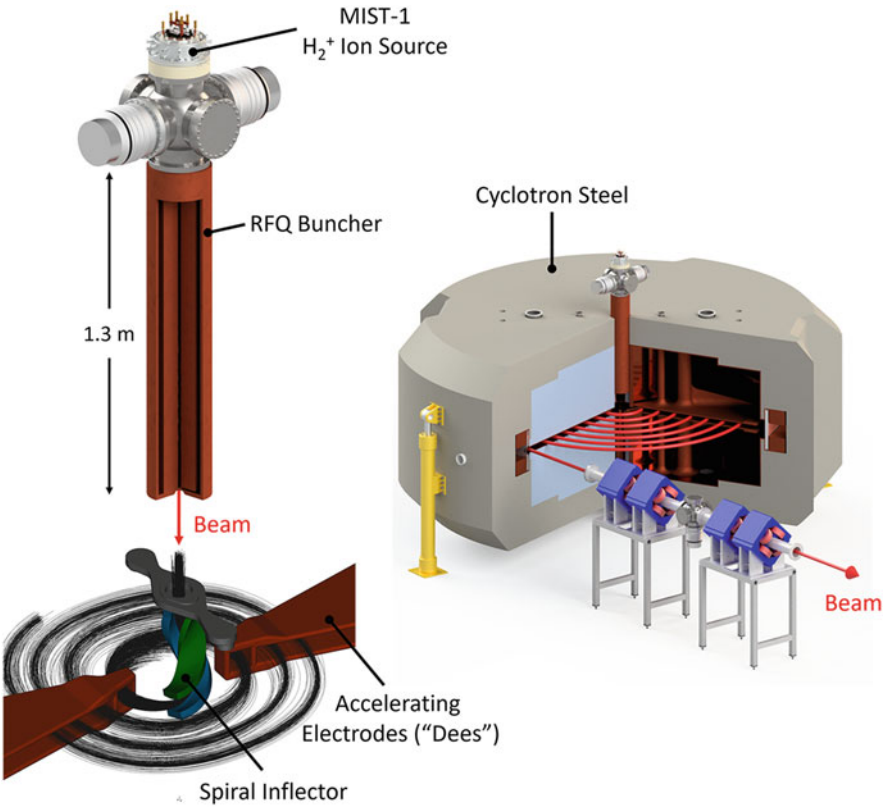

Fig. 8.5 The layout of the IsoDAR 60 MeV cyclotron and its input stage: H_2^+ source, RFQ and inflector. The same layout is to be used as an input stage for the DAEδALUS project (see Sect. 8.4.3)

reactor detectors. These detectors RENO50 [29] and JUNO [32] would be located ~50 km from the reactors. At this distance the disappearance of reactor $\bar{\nu}_e$'s is dominated by the solar Δm^2. However the additional small effect arising from the atmospheric Δm^2 is mass hierarchy dependent. A precise energy measurement of the IBD positron therefore allows the determination of the mass hierarchy, as well as more accurate measurements of θ_{12} and Δm^2_{12}.

The possibility to deploy a 10 kiloton liquid scintillator immersed off shore in the vicinity of a nuclear reactor complex in order to perform oscillation physics has been investigated [33]. This Hawai Anti-Neutrino Observatory, Hanohano, could alternatively be deployed far from a reactor in order to observe geological neutrinos.

Several scintillator detectors are also planned for deployment very close to reactors for neutrino oscillation into a sterile neutrino, accurate flux measurements and reactor monitoring, all using the IBD reaction. For this purpose they need to be compact. They also need to be segmented to mitigate the background from reactor

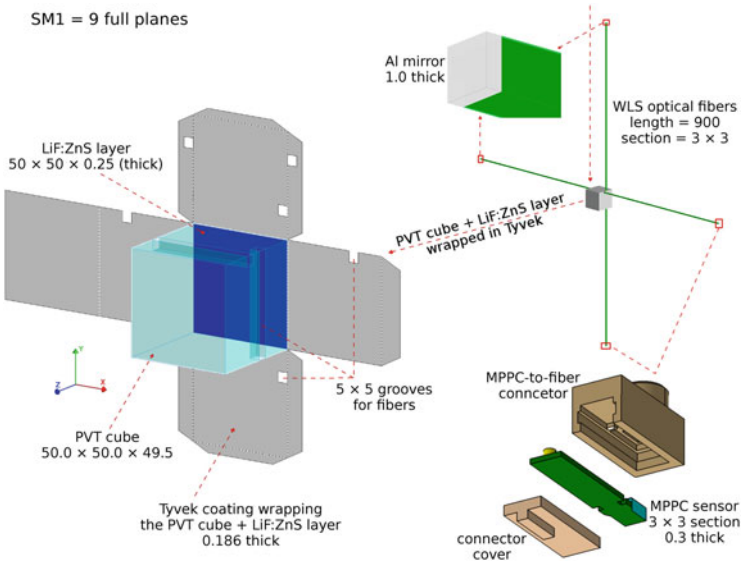

Fig. 8.6 An exploded view of a single PVT cube used in the SoLid detector prototype

neutrons. STEREO will use the same detector technique as described above for the θ_{13} experiments. Prospect [30] will run in 2 phases near a reactor at ORNL. Phase I will use a 3 ton single volume ^{6}Li loaded liquid scintillator detector movable between 7 and 12 m. The scintillator is EJ-309 from Eljen Technology to which ^{6}Li, PPO fluors and bis-MSB wavelength shifters have been added resulting in 6500 detected photons/MeV and a 4 m attenuation length. The volume is segmented by low mass optical separators into 120 segments 14.4 × 14.4 cm in cross-sectional area and 120 cm long, read by a pmt at each end. The positron deposits its energy in the liquid scintillator and the neutron is observed via its capture in hydrogen or ^{6}Li. The phase II detector will have a larger 10 ton mass while maintaining the same segmentation geometry and cover baselines between 15 and 19 m. Another example is the 1.6 ton SoLid built after prototyping a 288 kg version [31] deployed near the Belgian BR2 reactor. The final detector is built out of 12,000 $5 \times 5 \times 5\,\text{cm}^3$ ELJEN Technology EJ-200 polyvinyl toluene (PVT) cubes, Fig. 8.6. Sheets of ^{6}Li:ZnS(Ag), 225 µm thick allow the detection of the IBD neutrons through break up of the lithium to an alpha and ^{3}H with a Q-value of 4.78 MeV. The signals of each cube are read through two wave length shifting fibres connected to Hamamatsu S12572-050P multi-pixel photon counters.

Borexino [34] is a detector installed in Italy at the Laboratorio Nazionale del Gran Sasso (LNGS) for the measurement of solar neutrinos and in particular the ^{7}Be 862 keV monochromatic line using the purely leptonic reaction $\nu + e \rightarrow \nu + e$. This reaction results in an electron spectrum with a sharp edge at 665 keV. Borexino consists of 300 tons of liquid organic scintillator (pseudocumene and $1.5\,\text{g} \cdot \text{l}^{-1}$ PPO as fluor) housed in a nylon vessel itself suspended in a stainless

steel sphere on which are mounted 2200 photomultipliers. The sphere is filled with a pseudocumene solvent with a quencher acting as a shield for radioactivity coming mainly from the tubes and is itself immersed in a water Cerenkov tank viewed by an additional 200 photomultipliers to identify cosmic ray muons. The light yield of the detector is 500 photoelectrons/MeV actually recorded. Timing information from the photomultipliers allow the spatial reconstruction of the event and hence the determination that it occurred within the fiducial volume. The α and β^+ components of natural radioactivity can be reduced by pulse shape discrimination whereas the β^- and γ components are indistinguishable from the signal. A reduction and thorough understanding of the background has allowed them to observe solar neutrinos with an energy as low as 150 keV and, hence, make the first direct observation of pp fusion solar neutrinos as well as measure the solar beryllium line and geoneutrinos [35]. After a year during which the background has been reduced through six cycles of water extraction the radiopurity levels are now 2.7×10^{-18} for $^{14}C/^{12}C$ and, at 95% CL, $<9.7 \times 10^{-19} g \cdot g^{-1}$ for uranium and $<1.2 \times 10^{-18} g \cdot g^{-1}$ for thorium. This will allow improved measurements of solar and geoneutrinos as well as a new very short baseline neutrino oscillation project, SOX [36].

SOX is intended to search for oscillations of decay ν_e or $\bar{\nu}_e$ from a radioactive source into sterile neutrinos at the level of Δm^2 of 1 eV^2. The sources being considered are ^{51}Cr and ^{144}Ce, with the latter already approved. The ^{144}Ce would be placed in a pit under the Borexino detector. The small size of the 3.7–5.0 PBq source (about 1 L) coupled with the large 7 m size of the detector and its good spatial resolution of 12 cm and energy resolution of 3.5% would allow the observation of oscillation waves as a function of L/E within the detector as well as an overall measurement of $\bar{\nu}_e$ disappearance. Given an existing detector, the most taxing task is the source. It would be produced in a Russian laboratory from the reprocessing of nuclear fuel and must then be extensively shielded and transported to the Gran Sasso by a circuitous route for safety reasons.

Totally active liquid scintillator detectors have also been used in accelerator experiments producing higher energy neutrinos. MiniBooNE [37], looking for $\nu_\mu \rightarrow \nu_e$ oscillations in the Fermilab Booster neutrino beam in order to investigate the LSND signal [38], is exposed to neutrinos of about 1 GeV. The detector consists of 800 tons of mineral oil (CH_2) held in a spherical tank. The density of the oil is $0.86\, g \cdot cm^{-3}$ and has an index of refraction of 1.47. The light attenuation in this medium varies from a few cm at 280 nm to 20 m at 400 nm. The inner region (575 cm radius) is viewed by 1280 8-inch photomultipliers held on an optical barrier that separates it from a 35 cm thick outer region. This outer region, itself viewed by 240 tubes is used to veto events caused by charged particles entering the detector and to tag events that include particles exitting the detector in order to identify contained events. Cosmic ray events are greatly reduced by restricting the triggers to those occurring within a 19.2 µs window starting 4.4 µs before the 1.6 µs long beam spill. The energy of an event is related to the total amount of light observed. ν_μ and ν_e events are identified by the flavour (muon or electron) of the lepton in the final state CC interaction. Muons are distinguished from electrons using the light pattern of their Cerenkov rings as shown in Figs. 8.7 and 8.8. Muons give a sharp ring filled on

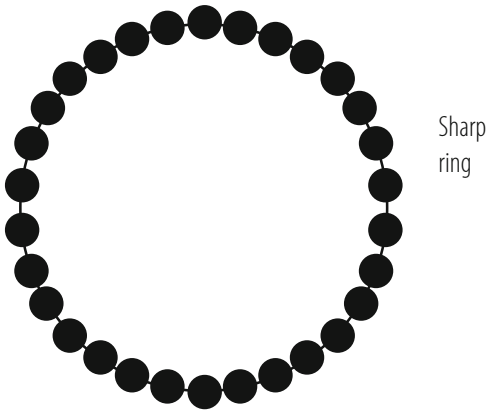

Fig. 8.7 The Cerenkov light pattern characteristic of a muon in the MiniBooNE detector

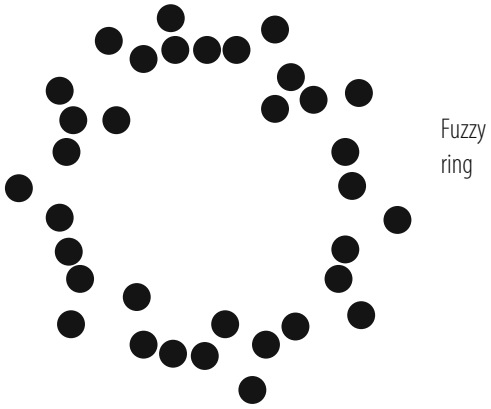

Fig. 8.8 The Cerenkov light pattern characteristic of an electron in the MiniBooNE detector

its interior as the muon approaches the tubes. Electrons give a fuzzy ring because of the many electrons and positrons each moving in a slightly different direction within the showers. In addition to the intrinsic ν_e component of the beam caused by μ, K and π decays the background to the ν_e appearance search comes from π^0 decays to two photons. This background can be greatly reduced by the ability of the detectors to observe separately the two electron-like rings produced by the two photons. The π^0's can be reconstructed with a mass resolution of 20 MeV/c^2. The event vertex, direction and energy resolutions with which ν_e events are reconstructed are 22 cm, 2.8° and 11% respectively. The experiment observed an unexplained excess of electromagnetic low energy events, but was not able to determine whether they were due to single photons or electrons due to the similarity of the rings produced by them.

Liquid scintillator detectors can also be of a tracking kind, in which the scintillator is confined in tubes and read by wave length shifting (WLS) fibres. NOvA [39], an experiment that runs in the Fermilab 2 GeV off-axis NuMI beam at a distance of 810 km from the lab is such an example. It consists of planes of extruded PVC tubes alternating in the horizontal and vertical direction. Each tube is 3.87 cm by 6 cm in cross-sectional area, 15.6 m long and is filled with mineral

oil with 5% pseudocumene. Since one of its physics goals is ν_e appearance it must be fine-grained enough to identify electrons and distinguish them from the showers produced from the decay photons of π^0 mesons. To this end, each plane corresponds to a sampling frequency of only 17% of a radiation length. The WLS fibres are in the shape of a loop and are read at the end opposite the loop. Avalanche photodiodes with a quantum efficicency of about 80% are used and detect 40 photoelectrons for a minimum ionizing particle crossing a tube at the far end. They are produced in arrays of 16 diodes each with a cross-section of $1.8 \times 1.0\,\text{mm}^2$ and must be run at a temperature of $-15\,^\circ\text{C}$. Each diode observes both ends of a fibre. The detector has an overall mass of 14 kilotons, consisting 70% of scintillator and the remainder of PVC. Its overall length is 67 m, with a cross section of $15.7 \times 15.7\,\text{m}^2$. The detector is located on the surface but the impact of cosmic rays is mitigated by the short beam spill of 10 µs and the speed of the photodiodes. Nonetheless, to reduce the electromagnetic component of cosmic rays, the detector is covered by a 3 m overburden of concrete and barite.

Totally active tracking detectors can also be made of extruded solid scintillator bars usually read with WLS fibres embedded in a hole or a groove made in the scintillator. An example of such a detector is SciBar [40], a 15 ton detector consisting of 14,336 strips each of dimensions $1.5 \times 2.5 \times 300\,\text{cm}^3$ and using 64-pixel multianode photomultipliers. It was first used in Japan on the KEK neutrino beam line and then moved to the NuMI beam line at Fermilab in the US.

Coherent Elastic Neutrino-Nucleus Scattering, CEνNS , is a process in which the neutrino interacts with the whole nucleus rather than with individual nucleons [41], leaving the nucleus whole and carrying very little energy since the momentum transfer must be small. The recoiling nucleus subsequently produces secondary recoils and scintillation light. The CEνNS cross section is several orders of magnitude larger than, for instance, the IBD cross section as it depends on the square of the number of neutrons in the nucleus. However, the smallness of the energy release made the process impossible to measure until recently. The COHERENT experiment [42] overcame this difficulty by using a 14.6 kg sodium-doped CsI crystal 34 cm long. The heavy cesium and iodine nuclei, provide the large cross sections and the large scintillation light yield necessary to detect low energy recoil nuclei down to a few keV. The crystal was read by a super bialkali low background Hamamatsu R877-100. The source of neutrinos was the decay of pions and muons produced by the Spallation Neutron Source at Oak Ridge National Laboratory. Protons on target(POTs) were delivered in 1 µs long spills at a rate of 60 Hz resulting in 4×10^{18} isotropically emitted neutrinos per day. The detector was placed in a basement corridor at a location, Fig. 8.9, that provided 12 m of neutron-moderating concrete and gravel in the direct line of sight to the SNS target, thus reducing neutron-induced recoil nuclei background (NIN) to an acceptable level. Cosmic rays were also reduced with an 8 m water overburden. The detector was enclosed in high-density polyethylene, to reduce NIN, as well as in both low activity and in standard lead. Muon vetos and water tanks containing a neutron moderator completed the shielding of the detector. The photomutiplier signals were amplified and digitized at 500 MSamples/s over 70 µs intervals starting 55 µs before the POT

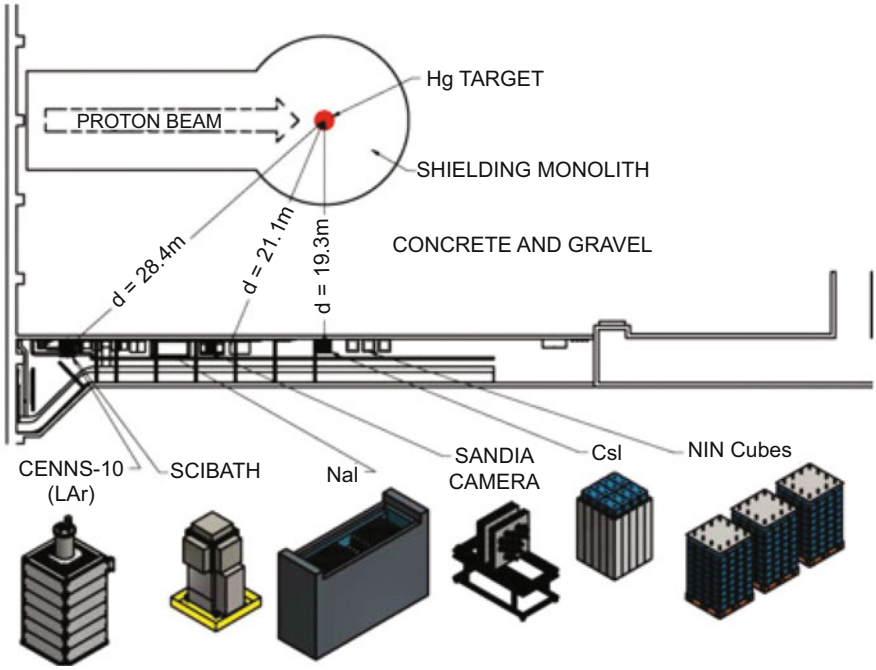

Fig. 8.9 The COHERENT experiment layout, showing the proton beam, target, shielding and experimental area

signal. Two 12 μs windows, one preceding and one following the POT trigger, allowed the comparison of data respectively unrelated and related to the beam. The 40 μs interval preceding these two windows was used to veto events due to previous energy depositions. The window following the POT signal showed a distribution of events consistent both in energy with coherent scattering and in time distribution with pion and muon decays. These signals were absent in the window preceding the POT, allowing the experimenters to announce a first observation of CEνNS at the 6.7 standard deviation confidence level. Detectors with different technologies such as liquid argon and NaI[T1] crystals are currently installed in the same location with further expansions being considered.

8.3.2 Water Cerenkovs

These are large volumes of ultra-pure water in which charged particles produced in neutrino interactions are detected through the Cerenkov light they emit. The measurement and separation of electrons, muons and π^0's is as was described in the context of MiniBooNE and illustrated in Figs. 8.7 and 8.8. Several experiments [43, 44], originally conceived to search for proton decay have pioneered this technique

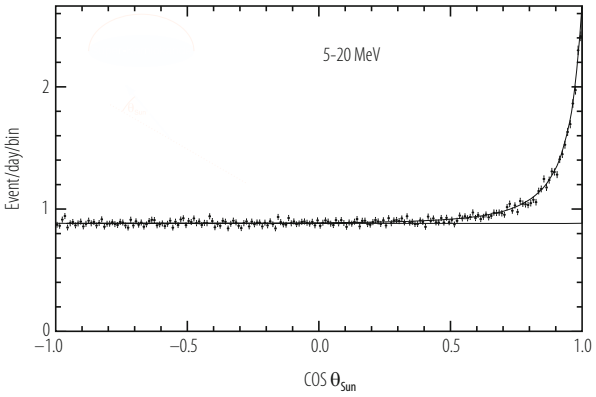

Fig. 8.10 The electron direction relative to the sun position in solar neutrino candidate events observed in SuperKamiokande

for the study of atmospheric and solar neutrinos, and, as a byproduct, have made the first recording of neutrinos emitted by a supernova, namely SN1987A. These detectors have been followed by the most productive one, SuperKamiokande(SK) [45], a 50 kiloton detector placed in the Kamioka mine in Japan at a depth of 2700 m water equivalent. It consists of two concentric cylindrical detectors. The inner one (ID) is viewed by 11,146 photomultipliers of 20 inch diameter providing a 40% coverage while the outer one(OD) is viewed by 1885 8 inch tubes. The absence of signal in the OD distinguishes fully contained events from partially contained ones. SK has successfully observed neutrinos ranging in energy from a few MeV(solar neutrinos) to several tens of GeV (atmospheric and accelerator neutrinos). The electron energy and direction produced in the elastic scattering reaction used to observe solar neutrinos are related to the incident neutrino energy and direction. The pointing accuracy is such that the origin of these neutrinos can be clearly associated to the sun, Fig. 8.10. In order to observe as much of the solar neutrino spectrum as possible, it has minimized background such as to be able to lower their detection threshold to ∼3.5 MeV. They have observed neutrino interactions coming from above and from below and have observed the reduction of ν_μ interactions from below (long baseline) due to $\nu_\mu \rightarrow \nu_\tau$ oscillations. Using a neural network approach they were also able to identify the resulting ν_τ CC component. SK is currently the heart of the T2K long baseline experiment [46] in which it is exposed to a beam of neutrinos or antineutrinos from the JPARC accelerator laboratory 295 km away. The beam is produced starting with 30 GeV protons and is an off-axis beam with a narrow neutrino energy spectrum peaked at 600 MeV. The experiment includes a near detector which will be described in Sect. 8.3.5. Their excellent electron and muon identification have allowed them to observe ν_μ disappearance as well as ν_e appearance, and measurements of $\sin^2\theta_{23}$, Δm^2_{23} as well as θ_{13}. In long baseline ν_e appearance experiments such as T2K or NOvA, the measured value of θ_{13} is correlated to the yet unknown CP violation phase, leading these experiments to

quote their measurement of θ_{13} as a range of values driven by the allowed CP phase values. Combining this range of θ_{13} with the precise reactor experiments measurement of θ_{13}, allows to limit the possible values of the CP violation phase.

Several long baseline projects based on the water Cerenkov technique have been proposed to measure the mass hierarchy and the CP phase via $\nu_\mu \rightarrow \nu_e$ oscillations. However because of the low signal event rate expected, detectors of the order of the megaton are needed. This would enable these detectors to continue the very successful non-beam physics programme of SK, namely atmospheric and solar neutrino physics, proton decay searches and supernovae watches. The MEMPHYS [47] project was planned in the context of a potential neutrino beam [48] from CERN to a new laboratory in the Frejus tunnel. It consists of 3 cylindrical water Cerenkov counters placed in contiguous caverns for a total of 0.5 megatons. Hyper-Kamiokande(HK), described in their Letter of Intent [49], is a natural extension of SK and would use the same beam as SK (600 MeV off-axis at 2.5°) but with its power upgraded from 0.75 MW to 1.35 MW, mostly by increasing the JPARC main ring repetition rate to 0.86 Hz. In their latest design the beam would impinge on a 0.52 Mton (0.38 Mton fiducial) water Cerenkov detector consisting of two 74 m diameter and 60 m high cylinders located 295 km from J-Parc in a cavern 650 m underground and 8 km south of SK. The Cerenkov light would be observed by 80,000 50 cm diameter Hamamatsu R12860 photomultipliers of a new Box and Line design providing 40% coverage with single photons detected with a 24% efficiency and a 1ns timing resolution. The photomultipliers have survived extensive pressure and implosion tests. Alternative sensors are also being investigated such as Hybrid Photo Detectors and the multi-photomultipliers concept developed for KM3Net [72]. The extrapolation of the water Cerenkov technique to a megaton-sized detector is driven to a large extent by the cost of the optical sensors and their production schedule, making the spacing and size of the sensors of prime importance. Similar detectors were considered for installation at SURF DUSEL [50] in order to observe neutrinos from a new beam from Fermilab. However, as will be discussed below, the liquid argon technique has been adopted instead.

A test [52] in the Super-Kamiokande detector demonstrated that neutrons from the IBD reaction $\bar{\nu}_e + p \rightarrow e^+ + n$ could be detected with the addition of gadolinium in the water. A 2.4 L acrylic vessel was filled with a 0.2% $GdCl_3$ mixture. A BGO crystal containing an Am/Be radioactive source was placed in its middle. The α particles emitted by the ameritium interacted in the beryllium via $\alpha + {}^9\text{Be} \rightarrow {}^{12}C^* + n$. By immersing the vessel in the SuperKamiokande detector and using the 4.43 MeV carbon deexcitation photon as a trigger it was demonstrated that the neutron could be detected via its absorption in the gadolinium, as described earlier in Sect. 8.3.1, with an efficiency of 66.7% with a 3 MeV threshold for delayed events. It was estimated that a background reduction of 2×10^{-4} could be achieved at a 10 MeV prompt event analysis threshold for $\bar{\nu}_e$. This opens the way for the use of the water Cerenkov technique for the detection of $\bar{\nu}_e$'s of geological or reactor origin.

Detectors that measured a deficit in the solar neutrino spectrum were all sensitive to ν_e only. In order to definitely prove that the deficit was due to a flavour

transformation rather than a disappearance it remained to prove that the overall flux of neutrinos, including all three flavours, was as predicted by the standard solar model. This was achieved by SNO [51] by measuring neutral current reactions which can occur for all three flavours since they do not have the energy constraint of charged currents, namely the mass of the appropriate produced charged lepton. It's heavy water (D_2O) target made it sensitive to three neutrino reactions, including neutral current reactions:

- Elastic scattering on electrons: $\nu_{e,\mu,\tau} + e^- \rightarrow \nu_{e,\mu,\tau} + e^-$
- Charged current absorption of neutrinos by deuterons: $\nu_e + d \rightarrow e^- + p + p$
- Neutral current disintegration of the deuteron with a threshold of 2.2 MeV: $\nu_{e,\mu,\tau} + d \rightarrow \nu_{e,\mu,\tau} + n + p$. This reaction could not be observed in light water because of the binding energy of oxygen being larger than the solar neutrino energies.The neutron was detected by absorption on deuterium or on ^{35}Cl in added $MgCl_2$. At a later stage of the experiment an array of ^3He filled proportional tubes was added providing a highly efficient neutron detection through the reaction $^3He + n \rightarrow p + {}^3H + 764\,\text{keV}$.

Because of the overall neutron production of only a few tens per day, care had to be given to select radiopure materials. The detector is located in a mine at a depth of 6000 m.w.e, thus reducing the cosmic ray background to 70/day. It consists of an acrylic sphere containing 1000 tons of heavy water viewed by 9438 photomultipliers. It is immersed in a structure containing light water for shielding and support. The proportional counters were placed in the heavy water in a lattice with 1 m spacing. The counters were 5.08 cm in diameter and filled with 85% ^3He and 15% CF_4 at a pressure of 2.5 atm. Electrons were detected by the Cerenkov light they emitted. These included those produced in the primary interaction as well as those produced through Compton scattering on electrons of photons emitted through neutron absorption.

Cerenkov detectors are also the technique of choice for cosmological neutrinos. The scarcity of these very high energy neutrinos requires the use of large naturally occurring target and detection media such as a lake [53] or sea water [54–57] or Antarctic ice [58, 59] which can be instrumented with photomultipliers at the scale of 1 km^3. The photomultipliers are connected into vertical strings and lowered in the water or, in the case of ice, into holes melted using hot water. The strings have to be located at great depths to shield the detector from downgoing cosmic muons. This necessitates the inclusion of the photomultipliers in pressure vessels. They must also be in regions of high light transmission in order to maximize the spacing of photomultipliers and reduce the cost. The most advanced of these detectors is ICECUBE [59] in the Antarctic. It consists of 86 strings positioned in a 125 m hexagonal grid at a depth between 1450 and 2450 m. Each string includes 60 digital optical modules (DOM). Each DOM is a 35 cm pressure vessel containing a 25 cm diameter pmt, a wave form digitizer, a fast ADC and electronics self-triggering at the level of 1/4 of a photoelectron. Digital information is sent to the surface. It is complemented by a 1 km^2 surface array consisting of 160 ice-filled tanks. The average absorption and scattering lengths of the ice at the detector depth are 110 m

and 20 m respectively at 400 nm. It's energy threshold is 100 GeV. A subarray, DeepCore, consisting of 8 strings closely spaced at 40–70 m and with a DOM separation of 7 m instead of 17 m allows the observation of neutrinos with energies as low as 10 GeV. ICECUBE can search for point sources with an angular resolution of 1.5°, based on the signal arrival time at the photomultipliers, which is also used to reject downgoing cosmic ray muons. ICECUBE made the first observation of cosmological neutrinos between 20 and 2000 TeV, at energies high enough that they could not be attributed to atmospheric neutrinos. Several extensions of ICECUBE are being considered. ICECUBE-Gen2 [60] consists of an additional 120 strings to augment the coverage by about an order of magnitude, coupled with new more directional sensitive detectors as well as smaller ones to reduce the hole diameter and hence the fuel cost. Another is PINGU [61], a proposal to study neutrino oscillations parameters using a sample of about 60,000 atmospheric neutrinos with a threshold energy of a few GeV obtained by instrumenting a 6 Mton clear ice volume at the bottom of ICECUBE with 26 closely spaced strings each carrying 192 optical modules.

In addition to optical detection of the Cerenkov light, Antarctic ice has also been used to detect the coherent radio signals emitted by the cascade resulting when a neutrino interacts in a dielectric medium, the ice. This kind of radiation was predicted by Askaryan [62] and is caused by propagating showers acquiring a negative charge excess through Compton scattering and the annihilation of positrons in the dielectric. When this excess moves at a velocity greater than the velocity of light in the medium, Cerenkov radiation will be emitted and will be coherent for wavelengths longer than the transverse dimension of the shower, corresponding to $\sim$1 GHz. The electric field strength will be proportional to the shower energy. The radio attenuation length has been measured to be about 1600 m at 300 MHz, making the ice suitable for widely spaced detectors. This technique has been applied using either detectors observing the ice from balloons and satellites or with detectors placed right on the ground. The first technique allows the observation of large volumes of ice but will have higher detection thresholds. The second, due to the proximity of the detectors to the ice will have lower detection thresholds but will be limited to smaller detection volumes. The ANITA [63], Antarctic Impulsive Transient Antenna experiment, is a good example of the first technique. It used a ballooon flying under the NASA Long Duration Balloon program at an altitude of 37 km which allows the observation of the whole antarctic ice sheet (1.5×10^6 km^2). It flew 3 times for 35, 31 and 22 days respectively and used horizontal and vertical polarization antennas with a band width of 200–1200 MHz. The data was read with 2 GSamples/s digitization resulting in a 100 ns waveform per channel and per trigger. ANITA has been able to set the best limit on neutrinos for energies greater than $10^{19.5}$ eV as well as finding no neutrino coincident within 10 min of any of 12 Gamma Ray Bursts (GRBs). A possible extension of this technique would be EVA [64], the Exa Volt Antenna project, which would lower the energy threshold by a factor of 10 using the inner surface of a super-pressure balloon as a toroidal reflector antenna 115 m in diameter.

ARA [65], the Askaryan Radio Array, is a ground based radio array using several stations of 16 antennas each embeded 200 m deep into the South Pole ice. Three stations are operational with two more being installed. Each station consists of four strings separated by 10 m and each consisting of a mixture of horizontal and vertical polarization antennas. The trigger requires 3 out of 16 signal to exceed a power threshold within 110 ns. So far, the deployed stations have found no neutrino candidate including a search centred on 57 GRBs. Ground arrays have also been proposed on the Ross Ice Shelf, (ARIANNA [66]) and in Greenland (GNO [67]).

This technique has also been extended to neutrino interactions in underground Rock Salt which allows for better shielding from cosmic rays and also to interactions in the loose layer of regolith sands on the moon surface. Both of these materials have attenuation lengths for radio waves of the order of 100 m. While the rock salt experiments use ground based detectors, the lunar ones, use various radio telescopes pointed at the lunar limb.The first lunar radio experiment was the Parkes Lunar Radio Cherenkov experiment [68] and was followed by LUNASKA [69], GLUE [70] which constrained the neutrino flux above 10^{21} eV and NuMooN [71] which constrained it above 10^{23} eV.

Following the good performance of ANTARES off Toulon in the Mediterannean, a northern hemisphere kilometer cube detector, KM3Net, is currently being implemented [72]. It will consist of two modules. ORCA, at the ANTARES site will consist of 115 closely packed strings in order to address neutrino oscillations and the mass hierarchy in the energy range 3–50 GeV. The site will have a diameter of 200 m and a height of 100 m. ARCA, off Capo Passero in Sicily, will consist of two blocks of 115 widely spaced strings each block having a diameter of 1 km and a height of 600 m. ARCA's physics objectives are neutrinos from extra terrestrial sources above 1 TeV and the origin of high energy cosmic rays. Each string of both modules will consist of 18 optical modules, each housing 31 7.5 cm diameter photomultipliers. These yield a photocathode area that exceeds by a factor of three that of a single 25 cm photomultiplier, provides some directional information and a good separation between one and two photoelectron signals.

Lastly a detector,GVD [73],the Gigaton Volume Detector is under construction at Lake Baikal to observe cosmological neutrinos. It will consist of eight 120 m diameter clusters of 8 strings each, each string carrying 36 optical modules housing a $10''$ Hamamatsu photomultiplier. The cluster separation is 300 m. It is planned to extend GVD to 18 clusters to make it a cubic kilometer detector.

A detector immersed in the sea in the gulf of Taranto had also been proposed [74] to study $\nu_\mu \rightarrow \nu_e$ oscillations in the then CNGS beam [75], the axis of which was at a height of 40 km above the surface, thus placing the detector in an off-axis location. In this case the array of photomultipliers consisted of a vertical plane facing the beam to observe Cerenkov light from the electrons and muons produced in charged current interactions and identify them from their light pattern.

8.3.2.1 Liquid Argon

The Liquid Argon Time Projection Chamber (TPC) is a detector technique that provides accurate imaging of interactions while providing a moderately dense medium ($1.4\,\mathrm{g}\cdot\mathrm{cm}^{-3}$) thus very suitable for neutrino physics. It consists, Fig. 8.11, of a volume of liquid argon sandwiched between a cathode and anode providing a drift field of the order of 500 V/cm. Charged particles traversing this volume ionize it and the resulting electrons drift to the anode. To improve the uniformity of the electric field, a field cage surrounds the volume between the cathode and anode and is constructed with hoop-shaped electrodes held at potentials that increase from the cathode to the anode. The anode consists of a succession of wire planes, usually two or three. The first planes encountered by the drift electrons are biased such as to prevent them from being captured. Signals in these planes are by induction only. The last plane actually collects the electrons. The wires of the different planes are at differing orientations to the vertical. Associating signals in the different wire planes according to their timing allows the reconstruction of two of the coordinates of the drift electrons and therefore of the track portion they originated from. The third coordinate, along the drift field, is obtained using the drift velocity ($\sim$1 mm/μs), and the time difference between the electron signal at the wire and the time of the neutrino interaction. The latter is in turn obtained from the timing

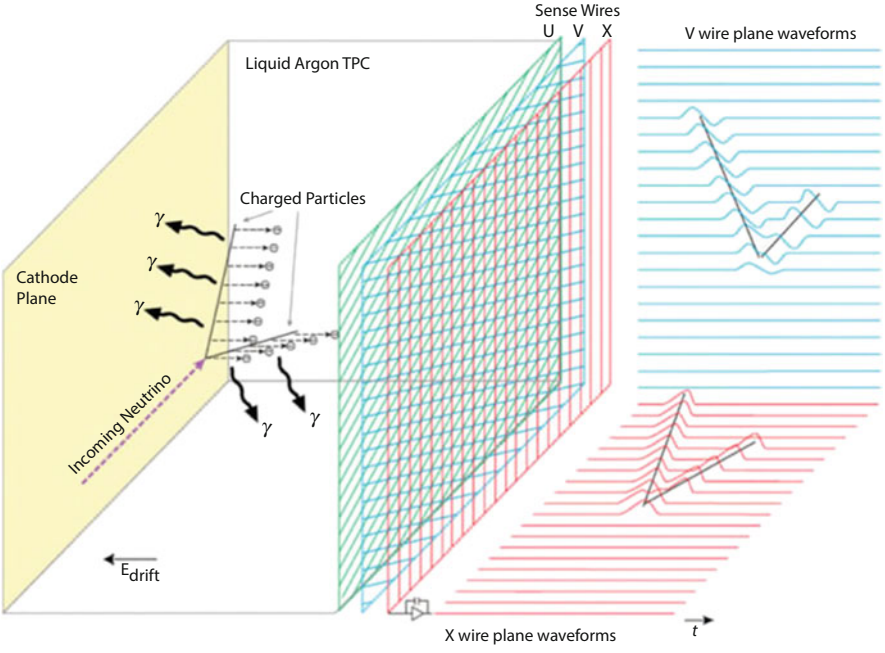

Fig. 8.11 The principle of signal recording in a Liquid Argon Time Projection Chamber as depicted in [78]

of the scintillation light emitted in the argon by the products of the interaction and recorded by photomultipliers. A track deposits energy along its trajectory and this is recorded as pulse heights in the wires. The pulse height distribution provides particle identification through the ionization pattern whereas the pulse height sum is a measure of the particle energy. The latter can also be obtained by range.

ICARUS [76], was the first to develop and use this technique. It was located at the Gran Sasso LNGS laboratory and was exposed to neutrinos produced by the CNGS beam 732 km away at CERN. It consists of two 300 ton modules each $3.6 \times 3.6 \times 19.9\,\mathrm{m}^3$. Each module includes a central high voltage plane and, along each of its long sides, three sets of detection wire planes, with orientation at 0° and ±60°. Electrons drift over a maximum distance of 1.5 m in the electric field perpendicular to the wire planes. This very complete detector relies on long drift distances and therefore requires high purity liquid argon. The purity achieved [77] during a technical run was such as to allow an electron drift lifetime of 1.8 ms equivalent to an electron mean free path of 280 cm. The electron drift velocity at 89°K increased from 0.5 mm/μs at an electric field of 0.1 kV/cm to 2 mm/μs at 1.0 kV/cm.

In the US, the first liquid argon TPC used in a physics experiment was ArgoNeuT [82], a 0.35 ton detector installed upstream of the MINOS near detector in the NUMI beam line at Fermilab. It produced significant low energy neutrino energy results as well as providing a test bed for subsequent larger liquid argon detectors.

The liquid argon technique has since been adopted for SBN [83], the Short Baseline Neutrino beam program at Fermilab, intended to investigate the possibility of additional, sterile, neutrinos. It uses the Booster Neutrino beam and consists of three liquid argon TPC detectors: SBND at 110 m from the neutrino source, MicroBooNE at 470 m and ICARUS at 600 m. The first to be installed was MicroBooNE [84], approved to observe electrons and photons and determine the origin of the low energy electromagnetic excess observed by MiniBooNE (Sect. 8.3.1). It's good spatial resolution would allow it to distinguish converting photon showers which are not associated to the primary vertex and are twice minimum ionizing at the conversion point from prompt electrons which are connected to the vertex and are singly ionizing. This should result in a good electron/photon discrimination. The TPC is inserted in a foam insulated cylindrical cryostat. It is 10.4 m long, 2.3 m high and 2.5 m wide. Electrons drift horizontally over a maximum of 2.5 m (corresponding to a maximum drift time of 2.25 ms) in a 0.273 kV/cm electric field and are recorded by two induction and one collection successive wire planes inclined respectively at ±60° and 0° to the vertical. The experiment was the first liquid argon TPC experiment to fill its cryostat without prior evacuation. It has achieved [85] an electron drift-lifetime of 18 ms corresponding to an O_2 equivalent contamination of 17 ppt and a loss of signal of 12% over the 2.5 m drift length. It also placed preamplifiers and shapers in the cold to reduce connection lengths and hence electronic noise. The amplified signals exit the cryostat and are digitized in warm ADCs before entering the DAQ electronics for Huffman compression and storage. This is done in two independent streams. The first stream records all the data occuring over

8 ms encompassing the trigger. This long recording time relative to the maximum drift time allows the complete reconstruction of cosmic rays traversing the TPC before or after the trigger but having part of their tracks reaching the wires during the event drift time. The second stream, intended for non-beam physics studies such as supernovae neutrinos, records all the data continuously but applies a zero suppression algorithm. Both the fast (6 ns) and slow (∼1μs) components of the argon ultra violet scintillation light are recorded by 35 Hamamatsu 5912-02MOD photomultipliers installed behind the anode wires and coated with Tetraphenyl Butadiene (TPB) to wave length shift the light from the ultra violet to the visible. The fast component is used to provide a trigger in time with the 1.6 μs beam spill and to tag cosmic ray tracks entering the detector during the event drift time. These are also tagged by a cosmic ray detector surrounding the cryostat and assembeled out of scintillation bars read by Kuraray WLS Y11 (200) S-type multiclad wave length shifting fibers and Hamamatsu S12825-050P multi-pixel silicon photomultipliers. A UV laser is used to map the TPC electric field, especially in the regions of non-uniformity caused by space charge effects. MicroBooNE has been collecting data since 2015. It has developed algorithms to distinguish between cosmic rays entering the detector at a rate of 4 kHz (because of its surface location) and neutrino interactions. It is also in the process of developing recontruction algorithms for electromagnetic showers that, at these low energies, can include gaps due to the propagation of low energy photons. Nonetheless liquid argon provides a remarkable visualization of events as depicted in Fig. 8.12. MicroBooNE is employing a Deep Learning technique [86] called semantic segmentation for the identification of the various classes of interactions.

The second detector to be installed will be ICARUS refurbished under the WA104/NP01 programme [87] at CERN. The following improvements were made to the detector:

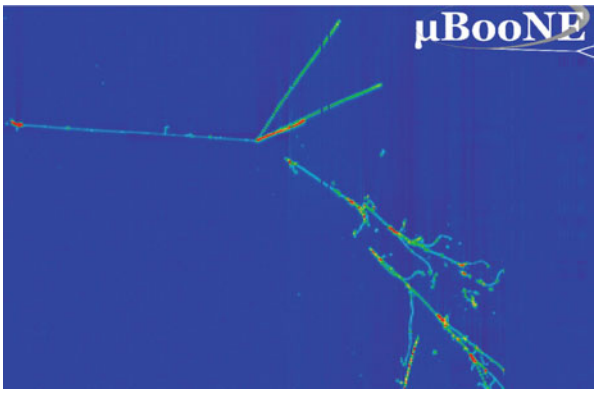

Fig. 8.12 A MicroBooNE Neutrino intearction event, showing charged particle tracks originating at the vertex and two photons, probably from a pizero, converting away from the vertex but pointing back to it

- The cathode plane was rebuilt to correct for up to 5 mm non-planarity.
- The optical system was upgraded to 360 8″ Hamamatsu 5912-mod (10 stage) cryogenic photomultipliers with TPB coating their face and read out by the CAEN V1730B 500 MHz 14 bit ADC system. The speed of this readout should allow the correlation of beam events with the Booster RF substructure, namely 1.15 ns pulses separated by 19 ns. If achieved, this correlation will reduce further the contamination of cosmic rays.
- The TPC electronics was modified as follows. The analogue signal shaping time was reduced to 1.5μs to match the electron transit time between wire planes and reduce undershoot in induction. Serial ADCs as well as a serial bus architecture with optical links were adopted. The feedthrough flange was used as the electronics backplane.

The third detector, SBND, described and referred to as LAr1-ND in [83], is a detector intended to measure the intrinsic beam composition, in particular of ν_e, before oscillations can occur. However its closeness to the neutrino target ensures a large number of neutrino interactions and hence a rich cross-section measurement programme. Its dimensions are 5 m along the beam, 4 m in height and 4 m laterally. The electrons drift along this latter dimension which consists of two 2 m drift spaces placed side by side. The Cathode Plane Assembly, CPA, is located in the middle and one Anode Plane Assembly, APA, is placed on either side and consists of the same number of wire planes and orientation as MicroBooNE. Each APA is made up of two 2.5 m wire frames along the beam but the U and V wires are connected to ensure continuous coverage. Unlike MicroBooNE, the ADCs will be in the cold together with the front end pre-amplifiers and shapers. The digitized signals will be multiplexed out of the cryostat via an FPGA. This will reduce the electronic noise and reduce the size of feed throughs. Upon exitting from the cryostat the signals will be converted to optical signals and sent, over optical fibres, to the warm DAQ electronics which will be identical to the one used by MicroBooNE. A 100 kV high voltage will provide a 500 V/cm drift field, the uniformity of which will be ensured by a field cage constructed with roll-formed tubes. A cosmic ray tagger of similar construction to the MicroBooNE one and a membrane cryostat will encase the detector. The light detection sytem will use the same pmt type and readout system as ICARUS. SBND will pioneer several detector concepts such as APAs and CPAs intended to be applied to the DUNE detector.

The liquid argon technique has been chosen for DUNE [88], the Deep Underground Neutrino Experiment $\nu_\mu \rightarrow \nu_e$ oscillation search intended to determine whether CP is violated in the neutrino sector and to measure the mass hierarchy. It will also address non-neutrino beam physics such as potential supernovae, proton decay and nnbar oscillations. The liquid argon technique was chosen instead of that of water Cerenkov for its good electron/photon discrimination resulting in a higher electron efficiency and therefore the possibility to use a smaller detector to achieve the same sensitivity. DUNE will be located 1475 m underground at SURF [89], the Sanford Underground Research Facility, in Lead, South Dakota and will be observing neutrinos produced at Fermilab 1300 km away. It will consist of four

TPC modules each containing 17,000 tons (10,000 tons fiducial volume) of liquid argon. The construction of the first module will follow the APA, CPA concept being tested in SBND, the so-called single-phase (liquid) approach. Its TPC dimensions are 12 m high, 14.5 m wide and 58 m along the beam. Three rows of APAs will be interleaved with 2 rows of CPAs, all oriented parallel to the beam. The APA-CPA horizontal separation, or drift length, will be 3.6 m, necessitating a 180 KV high voltage system for a 500 V/cm drift field. Each row of APAs consists of 25 vertically stacked pairs. Each row of pairs of facing APA-CPA is surrounded by a field cage. An APA consists of 4 wire planes separated by 4.76 mm with biases of -655 V, -365 V, 0 V and $+860$ V and orientation of $0°$, $+35.7°$, $-35.7°$ and $0°$ respectively. The wire separation is 4.7 mm. The TPC data is continuously digitized at 2 MHz by cold ADCs, serialized and transferred out of the cryostat on 12,000 high speed links per 10 kton module. They are received by Reconfigurable Computing Elements (RCEs) that buffer the raw data, zero-suppress it and pass it on to the trigger. While the zero-suppressed data is kept for non-beam physics, a second pass collects the full data set in regions of interest selected by the trigger. The photon detector system consists of light guides (2.2 m long, 83 mm wide and 6 mm thick) coated with TPB. The UV scintillation light impacting on the surface is re-emitted inside the bar at 430 nm and internally reflected in the guide to reach 12 SensL Cseries 6 mm^2 SiPMs. Ten such devices are mounted on each APA.

The second module will introduce a novel concept, the dual-phase approach first studied in [79] and tested as described in [80], in which the drifting electrons exit the liquid and are amplified in gaseous argon above the liquid. The concept is illustrated in Fig. 8.13 depicting the design of the dual phase prototype, ProtoDUNE-DP [81], currently under test at CERN. The DUNE dual phase module will consist of a 12 m wide, 12 m high and 60 m long homogeneous volume TPC. The electrons drift vertically over a maximum of 12 m in the 500 V/cm field provided by a segmented cathode at the bottom, the anode readout at the top and 60 stacked horizontal rectangular field rings. The reduction of the number of drift electrons reaching the wires due to absorption over the long drift space is compensated by the amplification in the gas. A 2 kV/cm field between a grid located just below the surface of the liquid and the Large Electron Multipliers (LEMs) charge amplification devices, causes the electrons to be extracted. The LEMs consist of a 1 mm thick printed circuit board with a micro-pattern of holes through its thickness and with one electrode on the top and one on the bottom surfaces. A 3 kV potential difference between the two electrodes results in a high field in each hole and the amplification of electrons entering them by about an order of magnitude through an avalanche process. The charge is collected in a two-dimensional x, y readout plane above the LEMs.

The technology of subsequent modules will depend on the performance of the single phase and double phase prototypes currently being built and tested at the CERN neutrino platform. DUNE also plans to use a near detector located close to the Fermilab neutrino source.

The addition of a magnetic field to a liquid argon detector would greatly enhance its capabilities. This has been tested [90] with an 11 L chamber placed in a 0.55 T magnetic field and the drifting properties were found to be preserved. However

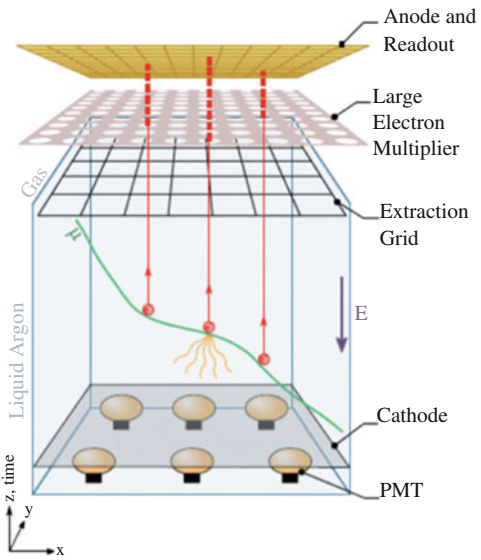

Fig. 8.13 The design of the ProtoDUNE dual phase prototype under test at CERN, showing the various components of the detector and, in particular, the amplification LEMs at the anode

measuring the charge and momentum of electrons would be challenging due to the short, 14 cm, radiation length of liquid argon resulting in only the first few cms being useful for magnetic measurements.

8.3.3 Calorimeters

These detectors are well suited to investigations requiring a measure of the total energy of an event rather than energy measurements of individual particles other than muons.

8.3.3.1 Iron-Scintillator

The CDHS detector [91] was used in the CERN SPS neutrino beam to study neutrino interactions in the energy range 30–300 GeV. It consisted of magnetized iron modules built from alternating layers of iron and scintillator and separated by drift chambers for a total of 1250 tons. Each module was constructed of circular iron plates 3.75 m in diameter and with a 30 cm central hole for the coil insertion. The coil consisted of 30 turns and was powered at 1000 A resulting in magnetic field of 1.65 T on average. It was uniform to $\pm 1.5\%$ azimuthally and dropped by about 20% with increasing radius. Two types of modules were used. Seven modules used fifteen 5 cm thick plates and twelve modules used five 15 cm thick plates. The iron plates alternated with planes of eight 45 cm wide NE110 scintillators except for

the last four modules which used a single scintillator plane for triggering. The drift chambers were 4 m wide hexagons and drifted vertically or at $\pm 60^{\circ}$ to the vertical in order to resolve ambiguities. The average efficiency was typically 99.5% and the spatial resolution 0.7 mm, which was adequate given the contribution of multiple scattering in the iron.

NuTeV/CCFR [92] used at Fermilab for a similar range of neutrino energies, differed from CDHS in that the calorimeter was separate from the magnetic spectrometer used to measure muon momenta. The 690 ton calorimeter consisted of 168 $3 \times 3 \times 5.15$ cm steel plates instrumented with Bicron 517L scintillator oil counters placed every two plates and drift chambers every four plates. This was followed by the magnetized iron toroidal spectrometer with an inner diameter of 25 cm to accomodate the four coils and an outer diameter of 350 cm. It consisted of three sections each followed by a drift chamber and two additional drift chambers downstream of the last section for improved momentum resolution. An important feature of this experiment was that a calibration beam was available in situ to determine the response [92] of the detector to electrons, muons and hadrons. The hadronic resolution was $\sigma_E/E = 0.86/\sqrt{E(GeV)} \bigoplus 0.022$ with an absolute scale uncertainty of 0.43%. The muon scale uncertainty was 0.7%, dominated by the field map determination in the iron. NuTeV performed a precise measurement of $\sin^2 \theta_W$ necessitating the measurement of both neutral and charged current events. They discriminated between the two on the basis of event length defined as the number of scintillator planes with non-zero pulse height in an event.

The 5.4 kiloton, 31 m long MINOS detector [93], similar in concept to CDHS, consists of 486 2.54 cm thick iron plates interleaved with planes of scintillator strips read by wave length shifting fibres. It was exposed to the Fermilab NuMI beam and housed in the Soudan mine 735 km away from Fermilab. This detector is studying ν_μ disappearance and therefore the shape and magnitude of the beam energy distribution must be very well understood. To minimize its dependence on Monte Carlo calculations the experiment is equipped with a near detector, located 1015 m from the target, which measures the beam spectrum and composition before any significant oscillations can occur. A transfer matrix is then used to predict the flux at Soudan. The transformation does not depend simply on the inverse of the square of the distance to the detector as the near detector, being close to the target, is not exposed to an exact point source because of the finite (725 m) length of the decay tunnel. The extruded polystyrene scintillator strips are 4.1 cm wide and 1 cm thick and are read by a 1.2 mm wave-length shifting fibre housed in a groove. The fibres are read by multi-anode photomultipliers, structured as 16 pixel in the far detector and 64 pixel in the near one. The data is multiplexed to reduce the number of readout channels. The coil provides a toroidal magnetic field in the iron allowing the measurement of the momentum and charge of secondary muons.

8.3.3.2 Fine-Grained

CHARM II [94] was a detector designed to measure $\sin^2\theta_W$ in $\nu_\mu - e$ scattering. The scattered electron is produced very forward unlike background events arising from ν-nucleon events. A cut of $E\theta^2 \leq 1$ MeV and $\theta < 10$ mrad, where E and θ are the scattered electron energy and production angle to the beam direction was used to reject this background, necessitating a very good angular resolution. Hence, glass, a low Z material to minimize multiple scattering, was selected as target material. Each of the 420 48 mm thick glass plates was followed by a plane of 352 plastic streamer tubes with a 1 cm pitch. The wires were readout in digital mode and 18 mm wide cathode strips glued to the outside of the tubes in a direction orthogonal to the wires were readout in analog mode to provide a measure of the energy and centroid of the electron showers. Consecutive modules had their strip and wire orientations rotated by 90° and consecutive modules with the same orientation had their wire spacing shifted by half the wire pitch. A scintillator plane was inserted in the detector after every 5 glass plates. The total mass of the calorimeter was 692 tons covering a volume of $3.7 \times 3.7 \times 15.4\,\mathrm{m}^3$. An electron angular resolution, σ_θ/θ, varying between 15–20 (mrad)/$\sqrt{E(GeV)}$ over the 2–24 GeV energy range of the experiment was achieved[95] as well as a vertex resolution of about 22 mm. The ability to discriminate the electrons from $\nu_\mu - e$ scattering from background is demonstrated in Fig. 8.14. A muon spectrometer consisting of six of the CDHS modules followed the glass target and provided a momentum resolution of 14% at 20 GeV/c and an angular resolution at the vertex of 18 mrad/E(GeV).

8.3.4 Emulsions

Detectors based on the photographic emulsion technique have a sub-micron spatial resolution and are therefore the detector of choice when searching for secondary vertices related to charmed particles or τ leptons. Until recently, this technique was limited because of the difficulty in scanning the emulsion. However recent developments in fast microscopes have revived it. Although ν_μ disappearance in atmospheric neutrinos was widely believed to be due to $\nu_\mu \rightarrow \nu_\tau$ interactions, it needed to be demonstrated through ν_τ appearance in a ν_μ beam. This was undertaken, using emulsions, by E531 [96] at Fermilab and by CHORUS [97] at CERN. At the neutrino energy of these experiments the τ travels only about 1–2 mm. CHORUS, the more sensitive of the two experiments used a 770 kg emulsion target built out of plates consisting of a 90 µm plastic base holding 350 µm thick emulsion layers on either side. The target was divided into four stacks each one followed by three interface emulsion sheets and a scintillating fibre tracker. Other sheets of emulsions were interleaved between the stacks and were changed several times throughout the data-taking in order to be exposed to fewer tracks and therefore ease the track reconstruction in the bulk emulsion. The fibres (more than 1 million) were read out by 58 optoelectronic readout chains each consisting of four image

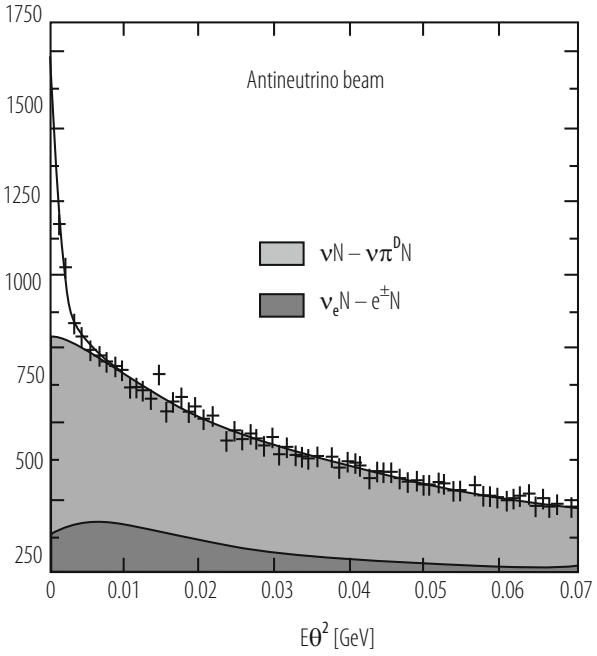

Fig. 8.14 The number of events as a function of $E\theta^2$, with E and θ respectively the scattered electron energy and direction as obtained during the antineutrino running of CHARM II, demonstrating the ability to identify electrons from $\nu_\mu - e$ scattering as evidenced by the sharp peak at small $E\theta^2$

intensifiers and a CCD camera. The target was followed by a hadron spectrometer including an air-core hexagonal magnet, an electromagnetic calorimeter and a muon spectrometer. The pulsed hexagonal magnet provided a momentum resolution varying between 20 and 50% in the momentum range 0–10 GeV/c. The scanning of the emulsions was made with fully automated Ultra Track Selector microscopes based on the track selector principle [98]. A series of tomographic images (Fig. 8.15) are taken in the emulsion at successive depths along the beam direction. Tracks then appear as aligned grains when the images are shifted according to track angle. Although they failed to find oscillations because of the kinematic region which they were sensitive to, E531 [100] and CHORUS [99] were successful in observing secondary vertices from a large sample of charm decays.

The search was then taken over by OPERA [102]. This experiment collected data at the LNGS laboratory using the CNGS beam. The long baseline of OPERA allowed the search for ν_τ appearance in the Δm^2 region then favoured by ν_μ disappearance. It used the emulsion cloud chamber technology as it is well suited to search for detached vertices or kinks over distances of the order of a mm. The 1766 ton detector was made up two supermodules. Each supermodule included 31 walls of bricks each 8.3 kg brick consisting of 57 plates of emulsions alternating

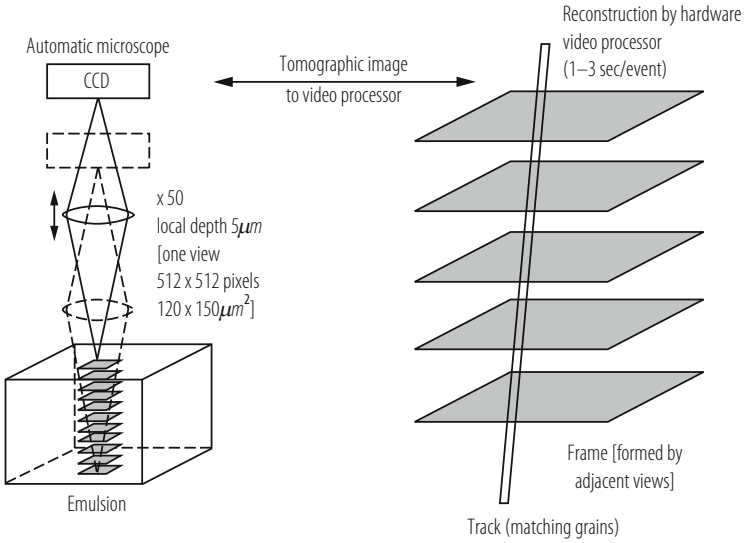

Fig. 8.15 The principle of tomographic scanning of emulsions

with 1 mm sheets of lead. An emulsion plate was made of two 44 μm emulsion sheets on either side of a 200 μm plastic layer. Each wall was followed by two planes of scintillator trackers one with vertical strips and one with horizontal strips. Each supermodule was completed with a magnetized iron muon spectrometer constructed with iron plates interleaved with resistive plate chambers and preceded and followed by 7 m long drift tubes. Bricks identified by the scintillator tracker as likely candidates for having been the site of a neutrino interaction were removed from the setup on a daily basis using a robot. They were briefly exposed to cosmic rays to provide sheet to sheet alignment and were then dismantled. The emulsions were developed and scanned. They observed [103] five ν_τ CC interactions through the detection of the resulting τ decaying to a single hadron in three events, to 3 hadrons in one event and to a muon in the fifth event. Their secondary vertex and kink detecting capability was again demonstated by their observation of neutrino generated charm events [104].

Emulsions were also used in DONUT [101], the first experiment to observe ν_τ interactions albeit from ν_τ's intrinsically present in the beam rather than from oscillations. In order to reduce the number of ν_μ and ν_e in the beam, the experiment used a neutrino beam produced by impinging the Fermilab proton beam in a 1 m long tungsten beam dump. Most pions and kaons that normally give rise to ν_μ and ν_e interacted before decaying, whereas the decay $D_s \rightarrow \tau \quad \nu_\tau$ followed by $\tau \rightarrow \nu_\tau + \ldots$ is fast enough to produce ν_τ's before the D_s interacted. This resulted in a neutrino beam with a 5% ν_τ content. Four emulsion targets were interleaved with scintillating fibre trackers. An electromagnetic calorimeter and a muon spectrometer completed the detector. Three types of emulsion targets were

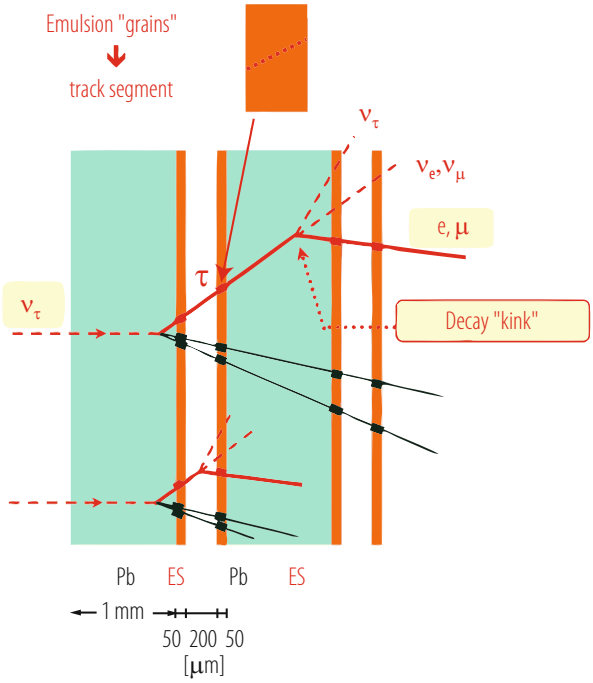

Fig. 8.16 The identification of secondary vertices using the emulsion cloud chamber technique described in the text

used. In order to increase the number of ν_τ interactions and reduce the amount of emulsion needed, in some of the targets DONUT used the emulsion cloud chamber technology, in which emulsion sheets are interleaved with lead or stainless steel plates as shown in Fig. 8.16. DONUT chose to use 1 mm thick stainless steel plates. In these targets, two types of emulsion plates were used: 100 μm emulsion sheets on either side of 200 μm or 800 μm plastic base. The remainder of the targets used bulk emulsion: 350 μm emulsion layers on either side of a 90 μm base. In the emulsion cloud chamber detectors the τ vertex is predominantly in the iron and therefore unobserved. But the precision with which the neutrino interaction vertex and the τ decay products can be reconstructed allows the identification of secondary vertices as described in Fig. 8.16. A plate to plate alignment accuracy of 0.2 μm over a $2.6 \times 2.6\,\text{mm}^2$ area was achieved by matching high momentum tracks in successive layers using position and direction information. This allowed a measure of the momentum of a particle using its multiple scattering, itself estimated using repeated changes of direction of the particle as it traverses the emulsion sheets.

This experiment also used external trackers to predict the position of interesting interactions in the emulsion. To facilitate this match each emulsion stack was followed by a changeable sheet, changed often to reduce its track density and facilitate the tracker-emulsion match. However it also used fast enough microscopes

to allow the use of stand alone techniques in which the emulsions were scanned without external information.

The latest scanning microscopes developed in Japan and Italy can measure at an average speed of 50 and 20 cm^2/h respectively. In addition to providing very precise spatial reconstruction emulsions, because of the large number of measurements along a track, can provide momentum measurements, as described above, and particle identification using ionization measurements, especially near the end point of stopping tracks. Please refer to Chap. 5 of this volume which addresses emulsion techniques in more details.

8.3.5 *Hybrid Detectors*

NOMAD [105] was a detector, Fig. 8.17, built to search for $\nu_\mu \rightarrow \nu_\tau$ oscillations by observing ν_τ interactions in the same ν_μ beam as used by CHORUS. However, unlike CHORUS, it intended to identify τ's not through the reconstruction of its separate decay vertex, but through kinematic criteria such as the missing transverse momentum arising from the unobserved neutrinos produced in τ decay. This demanded very good momentum resolution. The τ decay modes used in the analysis were $\tau^- \rightarrow \nu_\tau + hadrons$ and $\tau^- \rightarrow \nu_\tau + \bar{\nu}_e + e^-$. The latter mode was particularly useful as its main background is CC interactions of the intrinsic ν_e in the beam but this background is greatly suppressed because of the small ν_e contamination, $\sim$1%. However this mode did require very good electron identification. This latter

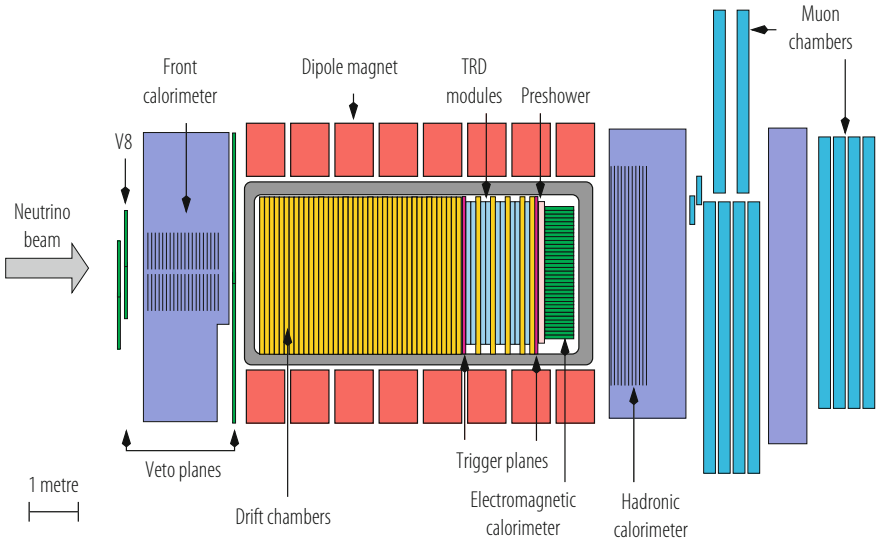

Fig. 8.17 The NOMAD hybrid detector used at CERN in the search for $\nu_\mu \rightarrow \nu_\tau$ oscillations

requirement as well as the requirement of good momentum resolution dictated the use of a light detector. The detector consisted of 49 drift chamber modules each one providing three coordinates with sense wires at 0°, +5° and −5° degrees to the vertical. The chambers were built out of honeycomb panels made of aramid fibres sandwiched between two kevlar skins. These panels provided the target material, 2.7 tons, for neutrino interactions. The average density of the target was $0.1\,\mathrm{g}\cdot\mathrm{cm}^{-3}$, close to that of a hydrogen bubble chamber and the drift chambers provided measurements every 2% of a radiation length (X_0). The spatial resolution was 150 µm providing a momentum resolution of $\sigma_p/p = \frac{0.05}{\sqrt{L}} \bigoplus \frac{0.008p}{\sqrt{L^5}}$, with the momentum p and the track length L expressed in GeV/c and meters respectively. The chambers were complemented by 9 modules of transition radiation detectors consisting of polypropylene foils and straw tubes containing an 80% xenon–20% methane gas mixture. These modules together with a 1.6 X_0 lead and proportional tube preshower and a 19 X_0 lead glass array provided the necessary e/π separation. These detectors were housed in a $7.5 \times 3.5 \times 3.5\,\mathrm{m}^3$ dipole magnet providing a 0.4 T horizontal magnetic field. The lead glass array, being inside the magnetic field, was read by tetrodes with a gain of 40 and had an energy resolution $\Delta E/E = (3.02/\sqrt{E(GeV)}+1.04)\%$. An iron-scintillator hadron calorimeter was located just outside the magnet coil and was followed by two muon detection stations consisting of large area drift chambers located after 8 and 13 interaction lengths.

Silicon is another technique that provides very precise track localization and hence, secondary vertex identification as has been proved repeatedly in hadronic interactions. NOMAD-STAR [106] was a 45 kg prototype of a possible application of this technology to neutrino interactions. It consisted of 4 plates of boron carbide providing the interaction mass interleaved with five planes of silicon detectors. Each plane consisted of ten 72 cm long ladders of 12 silicon-strip detectors with a pitch of 50 µm. It was exposed to a neutrino beam within the NOMAD detector and, in conjunction with the rest of the detector, it was able to reconstruct 45 charm decays. The hit to noise ratio was 17:1 and the hit finding efficiency 98%. The impact parameter resolution of the μ^- produced in a ν_μ CC interaction relative to a hadronic jet consisting of at least three charged particles was 33 µm.

The magnet used by NOMAD is now being used in the T2K experiment as part of the hybrid near detector [107] located 280 m from the target. The magnet houses:

- Scintillator planes interleaved with lead or brass optimized for photon detection and π^0 reconstruction.
- Three time projection chambers (TPC) using Micromegas modules for the drift electrons amplification and readout.
- These TPC's are interleaved with fine-grained detectors consisting of strips of scintillator providing target mass.
- A scintillator and radiator electromagnetic calorimeter.
- Scintillator planes housed in the slots located in the return yoke providing a muon range detector

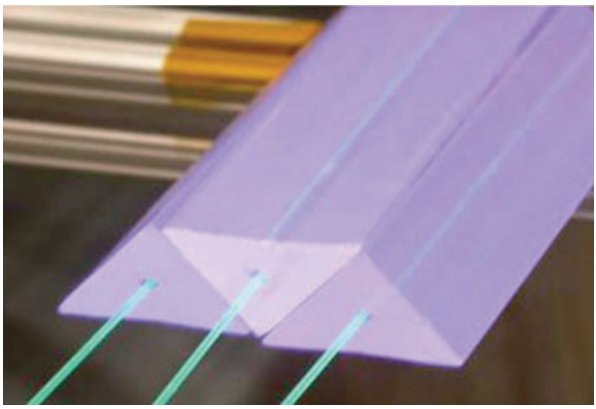

Fig. 8.18 The triangular scintillator strips and wave length shifting fibres of MINERvA

All scintillators in this near detector use Multi-Pixel Photon Counters as photosensors, a total of 50,000 channels. These are well suited as they operate in a magnetic field and provide single photon detection capability.

MINERvA, Main INjector ExpeRiment for ν-A, [108], an experiment to make precision measurements of neutrino cross sections using several nuclear targets (carbon, iron and lead) uses the NuMI beam at Fermilab and is located in front of the MINOS near detector. It consists of a fully active central detector surrounded and followed by electromagnetic and hadronic calorimeters. The central detector is built out of planes of 128 scintillator strips of triangular cross section, Fig. 8.18, and the electromagnetic and hadronic calorimeters use the lead-scintillator and steel-scintillator technology respectively. Wave-length shifting fibres are embedded in the scintillator strips and the light is channelled via clear fibres to multi-anode photomultipliers. Muons are identified and measured using the MINOS near detector. The overall cross section of the detector is hexagonal.

8.3.6 Radiochemical Detectors

Solar neutrino interactions are recorded by radiochemical experiments using the reaction: $\nu_e + (A, Z) \rightarrow e^- + (A, Z + 1)$. The atoms of $(A, Z + 1)$ produced are chemically extracted every few weeks, so this is not a real time process. They were first observed by the Homestake experiment [109] using ^{37}Cl producing ^{37}Ar. It was followed by three others, Gallex [110], Sage [111] and GNO [112], all of which used ^{71}Ga, changing to ^{71}Ge. Their characteristics are listed in Table 8.2. These experiments were housed underground to reduce cosmic ray background. In spite of the large flux of solar neutrinos on earth only a few such reactions occur

Table 8.2 Characteristics of the radiochemical solar neutrino experiments

	Homestake	Gallex	SAGE	GNO
Location	South Dakota	Gran Sasso	Baksan mine	Gran Sasso
Material	C_2Cl_4	Gallium (solution)	Gallium (metallic)	Gallium (solution)
Initial isotope	^{37}Cl	^{71}Ga	^{71}Ga	^{71}Ga
Detected isotope	^{37}Ar	^{71}Ge	^{71}Ge	^{71}Ge
Mass [tons]	615.0	30.3	57.0	30.3
Threshold	0.814 MeV	0.233 MeV	0.233 MeV	0.233 MeV
Extraction rate	3–4 months	3–4 weeks	3–4 weeks	3–4 weeks
Half-life of detection reaction	34 days	16.5 days	16.5 days	16.5 days

daily even for detectors weighing about a hundred tons due to the small neutrino interaction cross section at these low energies.

The Homestake experiment was located in the mine of the same name in South Dakota at a depth of 4200 m.w.e. The detector consisted of a cylindrical tank containing 615 tons of C_2Cl_4 and with 5% of its volume filled with helium gas at a pressure of 1.5 atmospheres. The argon produced was removed from the tank by bubbling helium through the tank and then trapping the argon in a cryogenically cooled charcoal absorber. Following several stages of purification the argon was transferred to a proportional counter after adding 7% of methane. The extraction efficiency was measured by inserting and extracting known amounts of either ^{36}Ar or ^{38}Ar. Because of the very low event rate possible radioactive contaminants in the tube material had to be minimized. The counters consisted of a highly refined iron cylindrical cathode and a 12–25 µm tungsten wire anode. The ^{37}Ar decays occur dominantly through K orbital electron capture depositing 2.82 keV of energy in the counter. This deposition is highly localized (100 µm) thus allowing it to be distinguished by pulse shape and rise time discrimination from background which is less localized.

Gallex and GNO, located in the LNGS, used 30.3 tons of Gallium containing 12 tons of ^{71}Ga in an aqueous solution acidified by the addition of HCl. This ensures that the ^{71}Ge produced is in the form of the highly volatile $GeCl_4$ in contrast with the non-volatile $GaCl_3$. The extraction procedure, as exemplified by that of GNO, is as follows [113]:

- The atoms of $GeCl_4$ (approximately 16 per 3–4 week run) are extracted into water by pumping nitrogen gas through the system.
- They are then converted into a gas, GeH_4 and mixed with Xenon.
- This mixture is introduced into proportional tubes 32 mm long and 6.4 mm in diameter made of ultrapure Suprasil quartz. The cathode consists of a single silicon crystal with impurities limited to $\leq$2ppt ^{238}U, $\leq$0.2ppt ^{232}Th and $\leq$0.1ppb ^{40}K. The anode is a 13 µm tungsten wire. The efficiency for transferring the

Germanium nuclei to the counters is measured to be 95–98% using non-radioactive Germanium carriers.
- X-rays occurring through the reactions $e^- + (A, Z+1) \rightarrow (A, Z) + \nu_e$ are detected over a period of about 6 months although the mean life of the reaction is only 16.5 days, allowing a good estimate of the background.
- The ^{71}Ge decays produce pulses of 10.4 keV or 1.1 keV for K and L captures respectively. The localized nature of this ionization allows the reduction of background using amplitude and shape analysis of the recorded pulses to a level of less than 0.1 event/day.
- The counters are calibrated 5 times during a 6-month exposure using a Gd/Ce X-ray source.

Gallex measured [114] their extraction efficiency using a 60 PBq ^{51}Cr source of 750 keV neutrinos (90%) and 430 keV (10%) neutrinos. They found a ratio of measured/expected signal of 0.93 ± 0.08. Their extraction efficiency was also confirmed [115] to be as expected to within 1% by introducing several thousand atoms of ^{71}As that decay to ^{71}Ge.

The SAGE detector was built using up to 60 tons of metallic Gallium. It was housed in the Baksan Neutrino Observatory in the Caucasus at a depth of 4700 m.w.e. While the liquid gallium was stirred at a rate of 80 rpm the Germanium was extracted from it by oxidizing it using a weakly acidic aqueous solution. The subsequent steps are similar to the procedure described above. Their extraction efficiency was also measured with a Chromium source.

The reaction threshold in chlorine only allows the observation of the beryllium and boron neutrinos whereas the threshold in gallium allows, in addition, the observation of some of the pp neutrinos.

8.3.7 Bubble Chambers

Bubble chambers were heavily used in earlier studies of neutrino interactions and were instrumental in making significant advances in the understanding of the properties of neutrinos [116]. Their filling varied from liquid hydrogen to heavy liquids, the latter used to increase the overall target mass, to contain the secondary hadrons produced and to convert photons. They were placed within a magnetic field in order to measure the momenta of the charged particles produced in the neutrino interactions. Their time resolution was poor as they were sensitive to all events occurring within a beam spill of typically millisecond duration. This could be improved by associating them to external electronic detectors.

Gargamelle was a cylindrical chamber 4.8 m long and 1.8 m in diameter. It was situated in a 2 T magnetic field produced by two coils. Neutral currents were first identified using this chamber [117] with a heavy freon (CF_3Br) filling resulting in a density of $1.5\,\mathrm{g \cdot cm^{-3}}$ and an interaction length of 58 cm. The identification of

neutral currents required the rejection of events containing muons in the final state. Muons were defined as satisfying one of the following categories:

- a particle leaving the visible volume without undergoing a nuclear scatter
- a particle which stops in the chamber and decays to an electron
- a negative particle stopping in the chamber without producing visible products (44% of negative muons are absorbed in the nucleus).

The hypothesis that the observed neutral current candidates could have been due to neutral hadrons entering the chamber was rejected as this would have resulted in a decrease of their number as a function of depth within the chamber, an effect that was not observed.

A 12-foot bubble chamber [118] (a $26\,\mathrm{m}^3$ cylinder) was used in the neutrino beam at the Argonne Zero Gradient Synchrotron (ZGS). It was the first chamber to use a superconducting magnet.

The superconducting technology was then used in subsequent bubble chambers. BEBC (the Big European Bubble Chamber) was a $33.5\,\mathrm{m}^3$ bubble chamber, Fig. 8.19, operating in a 3.5 T magnetic field and was exposed to the CERN neutrino beams. It was equipped with an External Muon Identifier (EMI) [119] consisting of proportional wire chambers placed behind an iron absorber and covering an area 6 m high and 25 m wide. A muon candidate track observed within the chamber was confirmed as a muon if, when its trajectory was extrapolated to the EMI, a hit was found within a distance consisting with multiple scattering. In order to reduce the miss-classification of events due to the random association of a neutral current event with a background muon in the EMI, an Internal Picket Fence [120] of proportional tubes placed between the chamber body and the magnet cryostat provided timing information for all events occurring within BEBC with a resolution of 230 ns full width. The tubes operated within the BEBC magnetic field. The chamber was used with fillings of liquid hydrogen, liquid deuterium or a neon-hydrogen mixture. This allowed the study of both νp and νn interactions. It was also used with a $3\,\mathrm{m}^3$ Track Sensitive Target (TST) which, when filled with hydrogen within a neon-hydrogen environment provided a sample of clean interactions within the hydrogen which could be compared to interactions in the neon for which nuclear effects had to be taken into account. In addition the heavier neon allowed a more efficient detection of secondaries.

The 15-foot bubble chamber at Fermilab ran in a magnetic field of 3.0 T. When filled with a neon-hydrogen mixture [121] (61.7% atomic neon and 38.3% atomic hydrogen) it provided a 23 ton target with a density of $0.75\,\mathrm{g}\cdot\mathrm{cm}^{-3}$, an interaction length of 125 cm and a radiation length of 40 cm. It was also fitted with an external muon identifier.

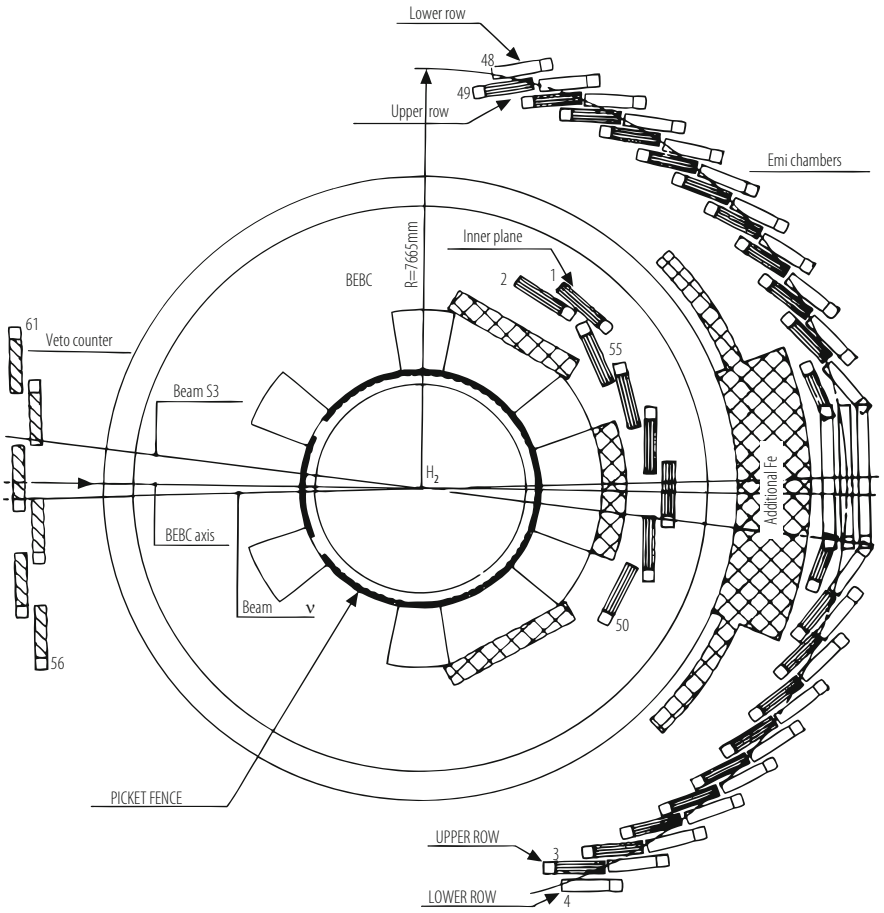

Fig. 8.19 The layout of the Big European Bubble Chamber (BEBC) including the External Muon Identifier and Internal Picket Fence

8.4 Ongoing Development Efforts on Neutrino Beams

Research based on neutrinos is currently proceeding along two paths. The first is focussed on completing our knowledge of the oscillation parameters by determining the mass hierarchy and searching for CP violation in the neutrino sector by comparing ν to $\bar{\nu}$ oscillations. The second avenue is determining whether sterile neutrinos exist. The first goal could be achieved with the presently planned detectors and beams described above. Nonetheless more accurate measurements would greatly benefit from higher intensity beams and much larger detectors. This has motivated several avenues of research pursued in the US and in Europe.

8.4.1 Beta Beams

Beta beams [122, 123] are beams of neutrinos based on the production, storage and β-decay of radioactive ions. A possible European solution was studied in the context of the Eurisol project [124]. ^{6}He ions which, decaying via β^{-}, produce ν_e and ^{18}Ne ions, which decaying via β^{+}, yield $\bar{\nu}_e$ would be stored. These ions would be accelerated to the energy required to produce decay neutrinos of the required energy and then stored in a race-track shaped storage ring. The Lorentz boost produces a well focussed forward beam which would illuminate one or more detectors in line with the straight sections of the storage ring. The search for CP violation would proceed by observing $\nu_e \rightarrow \nu_\mu$ and $\bar{\nu}_e \rightarrow \bar{\nu}_\mu$ oscillations. These oscillations would result in the observation of muons produced via the charged current interaction of ν_μ's and $\bar{\nu}_\mu$'s. These beams are particularly advantageous for the study of these oscillations as they do not, unlike present accelerator neutrino beams, have an intrinsic oscillated flavour component. Thus an important background is eliminated. The detector envisaged for this project was MEMPHYS, a water Cerenkov counter described in Sect. 8.3.2, located 130 km away from a potential beta beam source at CERN. This distance would require neutrino energies of a few hundred MeV to be at oscillation maximum. These low energies and distances would preclude any resolution of the mass hierarchy. As usual, an additional detector near the storage ring would be needed to study the beam before oscillations can occur. It is estimated that 2.9×10^{18} ^{6}He ions and 1.2×10^{18} ^{18}Ne ions decaying per year in the straight sections would be needed to meet the physics requirements. Whereas this seems achievable for ^{6}He, new production methods [125] would be needed for ^{18}Ne.

8.4.2 Neutrino Factory

A neutrino factory [126, 127] uses the decay of muons to produce neutrinos. The first step is to produce pions using a very high intensity proton beam impinging on a target. The decay of these pions then produce muons. Before they are injected into a storage ring their momentum and angular spread must be reduced to maximize their capture efficiency. This is done by phase rotation and ionization cooling. Longitudinal momentum spread would be reduced by phase rotation using the Neuffer scheme. This entails capturing multi bunches of muons with a very high Radio Frequency (RF) and rotating their phase with decreasing RF along the cooling channel. Angular spread (transverse momentum) would be reduced through ionization and subsequent longitudinal acceleration using RF cavities. The storage ring includes straight sections pointing to one or more detectors [129]. In the scheme studied in the context of the International Scoping Study [128] muons of both signs of about 20 GeV/c can be captured and stored simultaneously. Storage ring geometries have been identified that can deliver both neutrinos and antineutrinos to one or more detectors. In a race track geometry neutrinos and antineutrinos would

be identified in the same detector by time of arrival, itself related to the timing separation of μ^+ and μ^- bunches in the storage ring. In a triangular geometry two straight sections could point to two detectors. The physics envisaged with this project is the observation of $\nu_e \rightarrow \nu_\mu$ oscillations using the ν_e's produced in μ^+ decay. The signal is the observation of a μ^- as opposed to the copious μ^+'s produced by the interaction of the $\bar{\nu}_\mu$ also produced in μ^+ decay. The identification of the charge of these wrong sign muons necessitates the use of a magnetic detector. A 50 kton magnetized iron detector [130] coupled with scintillator or RPC's lends itself to this. Less dense detectors such as liquid argon TPC's and emulsion detectors [131] using the OPERA technology are also being considered to observe respectively electrons and τ leptons. These would allow the observation of additional oscillation channels which would be useful in removing ambiguities in the determination of oscillation parameters. With the higher energies and distances being considered the resolution of the mass hierarchy could be envisaged in addition to the search for CP violation.

The very high intensity proton beams needed to produce an adequate neutrino flux impose strong restrictions on the type of material used for the proton target. MERIT [132] is an R&D experiment at CERN intending to investigate the effectiveness of a mercury jet in a solenoidal field as a target. The constant flow of mercury would circumvent the problems related to stress and heating of a solid target. Muon cooling is being studied by MICE [133] at RAL with its strong synergy with MUCOOL [134] at Fermilab, with a setup including capture solenoids, liquid hydrogen absorbers and RF cavities. Incoming and outgoing spectrometers measure the effectiveness of the cooling.

8.4.3 High Current Cyclotrons

The present accelerator based long baseline experiments intend to compare oscillations of ν_μ to oscillations of $\bar{\nu}_\mu$. However the $\bar{\nu}_\mu$ beam has much more ν_μ background than the ν_μ beam has $\bar{\nu}_\mu$ background. This is because of the π^+ to π^- ratio at the proton target being larger than unity and because of the ν interaction cross section being larger than the $\bar{\nu}$ cross section. DAEδALUS [135] is an experiment aiming to remedy this situation by using the decay at rest of pions to produce a very pure source of $\bar{\nu}$ that would illuminate a detector also exposed to a long base line ν_μ beam. A beam of 800 MeV protons produced by a high current cyclotron impinges on a thick target producing pions which stop in the target, with the π^- being captured before decaying resulting in a beam dominated by the decay of π^+. As a consequence there will be essentially no $\pi^- \rightarrow \mu^- \rightarrow \mathrm{e}^- \nu_\mu \bar{\nu}_e$ and hence any $\bar{\nu}_e$ interaction observed must be from a $\bar{\nu}_\mu$ to $\bar{\nu}_e$ oscillation. The DAEδALUS project proposes installing three sources of pions at rest: one at 20 km from the detector which, for an average neutrino energy of 45 MeV, would be at the maximum oscillation probability and at the same L/E as the long baseline beam, one at 8 km to observe the rise in $\bar{\nu}_e$ appearance and one at 1.5 km for flux normalization.

The $\bar{\nu}_e$ would be observed through IBD for which a liquid argon detector as planned for DUNE would not be suitable. However, a water Cerenkov detector such as T2K or Hyper-K (especially if containing gadolinium to enhance the neutron capture rate as described in Sect. 8.3.2) or a large liquid scintillator detector would be ideal. As the flux out of the cyclotron would be continuous unlike the flux from the long baseline accelerator, the two sources of events would be distinguishable through absolute timing. The DAEδALUS collaboration is currently involved in increasing the current capability of cyclotrons to reach the 10 mA of protons necessary. The 800 MeV cyclotron would be superconducting, accelerate H_2^+ ions and would use as an injector the 60 MeV cyclotron described earlier in the context of IsoDAR. The H_2^+ ions would be stripped at extraction.

8.5 Conclusions

Neutrino detectors use the whole range of detector technologies available to high energy physicists. The smallness of neutrino cross sections necessitates the use of very large detectors that have ranged up to 50 kilotons when man-made and even 1000 megatons when using sea water or antarctic ice. The exception is the recent observation of coherent neutrino-nucleus scattering, a much larger cross section process, which allows the detection of neutrinos with smaller, albeit complex, detectors. Future generations of neutrino detectors to be used in conjunction with Very Long Base Line beams will address the oustanding questions in neutrino oscillation physics, namely the determination of the mass hierarchy and of CP violation in the neutrino sector as well as the determination of the possible existence of sterile neutrinos. In addition neutrinos are being used as probes. Ultra high energy (PeV) neutrinos originating in regions of space undergoing very violent processes are now beginning to be detected thus providing a new tool to study these processes. At the other end of the scale, neutrinos of a few MeV allow us to study the Earth and monitor reactors. These issues will require a whole range of detector sizes, up to the megatons, while at the same time requiring the precise measurements of the energies of electrons and photons and the identification of the secondary vertices of charmed particles and τ leptons. These detailed studies dictate the use of varied and complex detectors, thus ensuring that neutrino experiments will continue to use the very latest developments in detector technology.

References

1. http://www.ethbib.ethz.ch/exhibit/pauli/neutrino_e.html
2. Reines F *et al* 1953 Phys. Rev. **92** 830
3. Danby G *et al* 1962 Phys. Rev. Lett. **9** 36
4. Kodama K *et al* 2001 Phys. Lett. **B504** 218

5. Koshiba M 2008 Experimental results on neutrino masses and mixings, in Handbook of Particle Physics, Editor H. Schopper Landolt-Bornstein, Volume 1/12A
6. Camilleri L, Lisi E and Wilkerson J 2008 Neutrino Masses and Mixings: Status and Prospects Annu. Rev. Nucl. Part. Sci. **58** 343
7. Bahcall JN, Pinsonneault 2004 Phy. Rev. Lett. **92** 121301 and references therein.
8. Gaisser TK, Honda M 2002 Annu. Rev. Nucl. Part. Sci. **52** 153
9. Learned JG, Mannheim K 2000 Annu. Rev. Nucl. Part. Sci. **50** 679
10. Bemporad C *et al* 2002 Rev. Mod. Phys. **74** 297
11. Astier P *et al* 2003 Nuc. Instr. and Meth. **A515** 800
12. van der Meer S 1961 CERN Yellow Report **61-07**
13. Bernstein R *et al* 1994 Sign Selected Quadrupole Train FERMILAB-TM-1884
14. Yu J *et al* 1998 NuTeV SSQT Performance FERMILAB-TM-2040
15. Beavis D *et al* Long Baseline Neutrino Oscillation Experiment at the AGS (Proposal E889), Physics Design Report BNL 52459 (1995)
16. Dydak F 1980 Beam-Dump Experiments CERN-EP/80-204
17. Wachsmuth H 1979 Neutrino and Muon Fluxes in the CERN 400 GeV Proton Beam Dump Experiments CERN/EP 79-125
18. De Rujula A *et al* 1993 Nucl. Phys. **B405** 80
19. Apollonio M *et al* 2003 Eur. Phys. J. **C27** 331
20. Boehm F *et al* 2001 Phys. Rev. **D64** 112001
21. ExxonMobil https://ilrc.ucf.edu/documents/ILRC%2000000080/MSDS%2000000080.pdf
22. Ardellier E *et al* 2006 (Double Chooz Collaboration) hep-ex/0606025v4
23. Choi J H *et al* (RENO Collaboration) 2016 Phys. Rev. Lett. **116** 211801
24. An F P *et al* (Daya Bay Collaboration) 2016 Nucl. Instr. and Meth. **A811** 133
25. Choi J H 2016 Phys. Rev. Lett. **116** 211801
26. Abe S *et al* 2008 Phys. Rev. Lett. **100** 221803
27. Araki T *et al* 2005 Nature **436** 499
28. Alonso J R and Nakamura K (IsoDAR Collaboration) 2017 arXiv:1710.09325v1[physics.ins.det]
29. Joo K K (RENO and RENO50 Collaborations) 2017 J. Phys. Conf. Ser. **888** 012012
30. Ashenfelter J *et al* 2016 J. Phys.G:Nucl.Part.Phys. **43** 113001
31. Abreu Y *et al* 2018 arXiv:1802.02884v1[physics.ins.det]
32. Adam T *et al* (JUNO Collaboration) 2015 arXiv:1508.07166v2[physics.ins.det]
33. Learned J *et al* 2008 Hanohano: a deep ocean anti-neutrino detector for unique neutrino physics and geophysics studies. arXiv:0810.4975v1[hep-ex]
34. Alimonti G *et al* (Borexino Collaboration) 2009 Nucl. Instr. and Meth. **A600** 568
35. Derbin A and Muratova V *et al* (Borexino Collaboration) 2016 arXiv:1605.06795v1[hep-ex]
36. Bellini G *et al* 2013 arXiv:1304.7721v2[physics.ins-det]
37. Aguilar A A *et al* (MiniBooNE Collaboration) 2008 arXiv:0806.4201v1[hep-ex]
38. Aguilar A *et al* 2001 Phys. ReV. **D64** 112007
39. Ayres DS *et al* (NOνA Collaboration) 2005 arXiv:0503053[hep-ex]
40. Nitta K *et al* 2004 Nucl. Instr. and Meth. **A535** 147
41. Freedman D Z 1974 Phys. Rev. **D9** 1389
42. Akimov D *et al* 2017 arXiv:1708.01294v1[nucl-ex]
43. Bionta R *et al* 1983 Phys. Rev. Lett. **51** 27
44. Hirata KS *et al* 1988 Phys. Rev. **D38** 448
45. Fukuda S *et al* 2003 Nucl. Instr. and Meth. **A501** 418
46. Itow Y *et al* arXiv:0106019[hep-ex] and http://www2.phys.canterbury.ac.nz/~jaa53/presentations/Kato.pdf
47. de Bellephon A 2006 *et al* arXiv:0607026[hep-ex]
48. Gerigk F *et al Conceptual Design of the SPL II* CERN Yellow Report CERN 2006 -006
49. Abe K *et al* (Hyper-Kamiokande Working Group) 2011 arXiv:1109.3262v1[hep-ex]
50. The NSF multi-disciplinary initiative for a deep underground laboratory. http://www.lbl.gov/nsd/homestake

51. Boger J *et al* 2000 Nucl. Instr. and Meth. **A449** 172
52. Watanabe H *et al* 2008 arXiv:0811.0735v2[hep-ex]
53. Aynutdinov V *et al* 2008 Nucl. Instr. and Meth. **A588** 99
54. Aslanides E *et al* (ANTARES Collaboration) 1999 arXiv:9907432[astro-ph]
55. Carr J (ANTARES Collaboration) 2008 Nucl. Instr. and Meth. **A588** 80
56. Belias A (2007) in Proceedings of the First workshop on Exotic Physics with Neutrino Telescopes, EPNT06, page 97 arXiv:0701333[astro-ph]
57. Simeone F (On behalf of the NEMO Collaboration) 2008 Nucl. Instr. and Meth. **A588** 119
58. Ackermann M *et al* 2005 Astropart. Phys. **22** 339
59. Aartsen M G *et al* (IceCube Collaboration) 2017 JINST **12** P03012
60. Aartsen M G *et al* (IceCube-Gen2 Collaboration) 2014 arXiv:1412.5106v2[astro-ph.HE]
61. Aartsen M G *et al* (IceCube-Gen2 Collaboration) 2017 J.Phys. **G44** 054006
62. Askaryan G 1962 *Soviet Physics* JETP-USSR **14 (2)** 441
63. Gorham P W *et al* 2009 Astropart. Phys. **32** 10
64. Gorham P W *et al* 2011 Astropart. Phys. **35** 242
65. Allison P *et al* 2016 Phys. Rev. **D93** 082003
66. Barwick S W *et al* 2014 arXiv:1410.7369[astro-ph]
67. Wissel S A *et al* 2016 Published in PoS ICRC2015 1150
68. Hankins T H 1996 MNRAS **283** 1027
69. Bray J D *et al* 2015 Astropart. Phys.**65** 22
70. Gorham P W *et al* 2004 Phys. Rev. Lett **93** 041101
71. Buitink S *et al* 2010 Astron.Astrophys. **521** A47
72. Adrian-Martinez S *et al* (KM3Net Collaboration) 2016 J. Phys. **G43** 084001 and arXiv:1601.07459v2[astro-ph.IM]
73. Avrorin A D *et al* 2014 Nuc. Instrum. Meth. **A742** 82
74. Ball A E *et al* 2007 Eur. Phys. J. **C49** 1117
75. Acquistapace G *et al* 1998 CERN Yellow Report 98-02, INFN-AE-98-05
76. Amerio S *et al* 2004 Nucl. Instr. and Meth. **A527** 329
77. Amoruso S *et al* 2004 Nucl. Instr. and Meth. **A516** 68
78. Adams C *et al* 2018 arXiv:1802.08709v2[physics.ins-det]
79. Rubbia A 2004 arXiv:0402110[hep-ph] and http://neutrino.ethz.ch/GLACIER/
80. Badertscher A 2012 arXiv:1204.3530v3[physics.ins-det]
81. Manenti L (ProtoDUNE Collaboration) 2017 arXiv:1705.05669v2[physics.ins-det]
82. http://t692.fnal.gov/ ArgoNeut: Mini LAr TPC Exposure to Fermilab's NuMI Beam
83. Acciarri R *et al* 2015 arXiv:1503.01520v1[physics.ins-det]
84. A Proposal for a New Experiment Using the Booster and NuMI Beamlines: MicroBooNE 2007 Fermilab Proposal P974. and Acciarri R *et al* 2017 J.Inst **12** P02017
85. The MicroBooNE Collaboration 2017 MicroBooNE Public Note http://microboone.fnal.gov/wp-content/uploads/MICROBOONE-NOTE-1026-PUB.pdf
86. He K *et al* 2015 arXiv:1512.03385v1[cs.CV] and Ronneberger O *et al* 2015 arXiv:1505.04597v1[cs.CV]
87. Bonesini M (WA104 Collaboration) 2015 J. Phys.:Conf.Ser. **650** 012015
88. Acciarri R 2017 *et al* arXiv:1601.02984v1[physics.ins-det]
89. Heise J 2017 arXiv:1710.11584v1[physics.ins-det]
90. Badertscher A *et al* 2005 Nucl. Instr. and Meth. **A555** 294
91. Holder M *et al* 1978 Nucl. Instr. and Meth. **148** 235
92. Harris D A *et al* 2000 Nucl. Instr. and Meth. **A447** 377
93. Michael D G *et al* 2006 Phys. Rev. Lett. **97** 191801 and references therein
94. De Winter K *et al* 1989 Nucl. Instr. and Meth. **A278** 670
95. Geiregat D *et al* 1993 Nucl. Instr. and Meth. **A325** 92
96. Ushida N *et al* 1986 Phys. Rev. Lett. **57** 2897
97. Eskut E *et al* (1997) Nucl. Instr. and Meth. **A401** 7
98. Aoki S *et al* 1990 Nucl. Instr. and Meth. **B51** 466
99. Onengut G *et al* 2005 Phys. Lett. **B613** 105

100. Ushida N *et al* (E531 Collaboration) 1988 Phys. Lett. **B206** 375
101. Kodama K *et al* 2002 Nucl. Instr. and Meth. A **493** 45 and references therein
102. Guler M *et al* CERN SPSC 2000-028 SPSC/P318 LNGS P25/2000
103. Agafonova N *et al* (OPERA Collaboration)2015 Phys. Rev. Lett. **115** 121802
104. Agafonova N *et al* (OPERA Collaboration)2014 Eur. Phys. J. **C74** no.8 2986
105. Altegoer J *et al* 1998 Nucl. Instr. and Meth. **A404** 96
106. Ellis M, Soler FJP 2003 J. Phys. G: Nucl. Part. Phys. **29** 1975
107. Lindner T, 2008 Status of the T2K 280 m Near Detector. arXiv:0810.2220v1[hep-ex]
108. 2004 Proposal to Perform a High-Statistics Neutrino Scattering experiment Using a Fine-grained Detector in the NuMI Beam arXiv:0405002v1[hep-ex]
109. Cleveland B T *et al* 1998 Astrophys. J. **496** 505
110. Hampel W *et al* 1999 Phys. Lett. **B447** 127
111. Aburashitov J N *et al* 1999 Pys. Rv. **D60** 055801
112. Altmann M *et al* 2005 Phys. Lett. **B616** 174
113. Altmann M *et al* 2000 Phys. Lett. **B490** 16
114. Hampel W *et al* 1998 Phys. Lett. **B420** 114
115. Hampel W *et al* 1998 Phys. Lett. **B436** 158
116. Haidt D 1994 Nucl. Phys. (Proc. Suppl.) **B36** 387
117. Hasert FJ *et al* 1974 Nucl. Phys. **B73** 1
118. Barish SJ *et al* 1974 Phys.Rev.Lett. **33** 448
119. Brand C *et al* 1976 Nucl. Instrum.Meth. **136** 485
120. H. Foeth *et al*1987 Nucl. Instrum. Meth. **253** 245
121. Baker NJ *et al* 1989 Phys. Rev. **D40** 2753
122. Zucchelli P 2002 Phys. Lett.B **532** 166
123. Autin B *et al* 2003 J. Phys. G: Nucl. Part. Phys. **29** 1785
124. *European Isotope Separation Online* http://ganinfo.in2p3.fr/eurisol/
125. Rubbia C, Ferrar A, Kadi Y and Vlachoudis V 2006 Nucl. Instrum. Meth. **568** 475
126. Geer S 1998 Phys. Rev. D **57** 6989
127. De Rujula A, Gavela M B and Hernandez P 1999 Nucl. Phys. B **547** 21
128. Zisman M S (For the ISS Accelerator Working Group) 2008 J. Phys. Conf. Ser. **110** 112006
129. Abe T *et al* 2009 J. Inst. **4** T05001
130. Cervera-Villanueva A, MIND performance and prototyping, in the proceedings of the 9th International Workshop on Neutrino Factories, Superbeams and Betabeams-NuFact 07, editors O. Yasuda, C. Ohmori and N. Mondal American Institute of Physics, p 178.
131. Autiero D *et al* arXiv:0305185[hep-ph]
132. Bennett J *et al* CERN-INTC 2004-16
133. Kaplan D (For the MAP and MICE Collaborations) 2013 arXiv:1307.3891v1[physics.acc-ph]
134. Kochemirovskiy A *et al* 2016 in CNUM616-08-21 NuFact16 in Quy Nhon, Vietnam http://Vietnam.in2p3.fr/2016/nufact
135. Aberle C *et al* (The DAEδALUS Collaboration) 2013 physics.acc-ph arXiv:1307.2949v1 and Alonso J R 2016 arXiv:1611.03548v1[physics.acc-ph]